FEDERAL UNIVERSITY OF CEARÁ
CENTER OF TECHNOLOGY
DEPARTMENT OF ELECTRICAL ENGINEERING
UNDERGRADUATE COURSE IN ELECTRICAL ENGINEERING

SAMUEL ANTONIO MACEDO DE OLIVEIRA

MODELING OF POWER CONVERTERS EMPLOYING THE WCR-4SSC

FORTALEZA
2025

SAMUEL ANTONIO MACEDO DE OLIVEIRA

MODELING OF POWER CONVERTERS EMPLOYING THE WCR-4SSC

Undergraduate Thesis submitted to the Electrical Engineering Course of the Center of Technology of the Federal University of Ceará, as a partial requirement for obtaining the Bachelor Degree in Electrical Engineering.

Advisor: Prof. Dr. Dalton de Araújo Honório.

FORTALEZA
2025

Dados Internacionais de Catalogação na Publicação
Universidade Federal do Ceará
Sistema de Bibliotecas
Gerada automaticamente pelo módulo Catalog, mediante os dados fornecidos pelo(a) autor(a)

O51m Oliveira, Samuel Antonio Macedo de.
Modeling of power converters employing the WCR-4SSC / Samuel Antonio Macedo de Oliveira. – 2025.
62 f. : il. color.

Trabalho de Conclusão de Curso (graduação) – Universidade Federal do Ceará, Centro de Tecnologia, Curso de Engenharia Elétrica, Fortaleza, 2025.
Orientação: Prof. Dr. Dalton de Araújo Honório.

1. Conversores CC-CC. 2. Modelagem por variáveis de estado. 3. Conversor Cuk. 4. WCR-4SSC. I. Título.

CDD 621.3

SAMUEL ANTONIO MACEDO DE OLIVEIRA

MODELING OF POWER CONVERTERS EMPLOYING THE WCR-4SSC

Undergraduate Thesis submitted to the Electrical Engineering Course of the Center of Technology of the Federal University of Ceará, as a partial requirement for obtaining the Bachelor Degree in Electrical Engineering.

Approved on: 03/12/2025.

EXAMINATION BOARD

Prof. Dr. Dalton de Araújo Honório (Orientador)
Federal University of Ceará (UFC)

Prof. Dr. Fernando Lessa Tofoli
Federal University of São João del-Rei (UFSJ)

Eng. Pedro Herysson Almeida da Silva
Federal University of Ceará (UFC)

To my parents, Eduardo and Márcia, and to my entire family for their unconditional support during this journey.

ACKNOWLEDGEMENTS

To my parents, Eduardo and Márcia, for their love, affection, and support throughout my entire life.

To my great friend Cleomon, for his companionship throughout all these years and for his direct contribution to the development of this work through our conversations and reflections.

To my girlfriend Bruna, for her understanding and for the joy and peace she has brought into my life.

To the Computer Vision and Engineering Nucleus (NUVEN), for the freedom granted during the development of this work.

To my advisor, Prof. Dr. Dalton Honório, for the research opportunity he gave me at the beginning of my undergraduate studies, for his teachings and advice throughout my entire academic journey, and for his guidance on this work, bringing this cycle to a close.

To the examination committee members, Prof. Dr. Fernando Lessa Tofoli and Eng. Pedro Herysson, for accepting the invitation, for their valuable contributions, and for the time dedicated to reviewing this work.

"Para ser grande, sê inteiro [...] Põe quanto és no mínimo que fazes. Assim em cada lago a lua toda brilha, porque alta vive."

(Fernando Pessoa)

ABSTRACT

This work presents a generalized modeling methodology for the family of DC-DC converters based on the Four-State Switching Cell with a Wide Conversion Range (WCR-4SSC) operating in Continuous Conduction Mode (CCM). The core of the methodology relies on the state-space averaging (SSA) technique. A key contribution of this research is the simplification of the converter's six distinct switching stages into an equivalent two-stage model. This simplified model is governed by an equivalent duty cycle (d^{*}) that is dependent on the converter's specific operating region (R1, R2, or R3). A step-by-step procedure for deriving the averaged model and its subsequent linearization is established and applied in detail to the WCR-4SSC Ćuk converter as a representative example, resulting in the derivation of its complete set of small-signal transfer functions. To validate the proposed methodology, the derived analytical model (implemented in MATLAB) is compared against detailed circuit simulations (PSIM). The results demonstrate excellent agreement in both the frequency domain (Bode plots) and the time domain (transient responses). This confirms the model's accuracy across different operating points and validates the methodology as a robust and generalized foundation for the analysis and control design of all converters in the WCR-4SSC family.

Keywords: WCR-4SSC; DC-DC Converters; Modeling; State-Space Averaging; Ćuk Converter.

CONTENTS

1 INTRODUCTION 9

2 LITERATURE REVIEW AND MOTIVATION OF THIS WORK 11

2.1 Origin of the WCR-4SSC 11

2.2 Modeling and small-signal models 13

3 THE FOUR-STATE SWITCHING CELL WITH WIDE-CONVERSION RANGE 17

3.1 Study of the transformer 17

3.2 The cell 20

3.2.1 Region 1 21

3.2.1.1 1st Stage 22

3.2.1.2 2nd Stage 24

3.2.1.3 3rd-6th Stage 24

3.2.1.4 Equivalent Two-Stage Model 25

3.2.2 Region 2 26

3.2.2.1 1st Stage 27

3.2.2.2 2nd Stage 28

3.2.2.3 3rd-6th Stage 28

3.2.2.4 Equivalent Two-Stage Model 28

3.2.3 Region 3 29

3.2.3.1 1st Stage 30

3.2.3.2 2nd Stage 30

3.2.3.3 3rd-6th Stage 30

3.2.3.4 Equivalent Two-Stage Model 31

3.3 Summary 32

4 PROPOSED MODELING METHODOLOGY 33

4.1 State-space averaging technique 33

4.1.1 Theoretical background 33

4.1.2 Step-by-step procedure 36

4.2 Example: WCR-4SSC Ćuk Converter 37

5 RESULTS 41

5.1 Time-domain 41

5.2 **Frequency-domain** 43

6 **CONCLUSION AND FUTURE WORKS** 45

BIBLIOGRAPHY 46

APPENDIX A –MATLAB CODES 47

APPENDIX B –TRANSFER FUNCTIONS FOR CLASSICAL TOPOLOGIES (REGION 2) 54

APPENDIX C –PSIM SCHEMATIC 62

1 INTRODUCTION

Power electronic converters are a cornerstone of modern society, serving as the essential interface between electrical sources and loads. Their primary function is to efficiently convert and condition electrical energy, transforming voltage, current, and frequency to meet the specific requirements of an application. This capability is critical in countless systems, from the power supplies in personal electronics like smartphones and laptops to the industrial motor drives that power our manufacturing sector, the charging infrastructure for electric vehicles, and the uninterruptible power systems (UPSs) that support our critical data centers.

The role of power converters has become even more pronounced with the global shift towards renewable energy. Sources such as photovoltaic (PV) panels and wind turbines produce power that is intermittent and often incompatible with the electrical grid, generating variable low-voltage DC or variable-frequency AC. Power converters are the enabling technology that overcomes this challenge, stepping up low voltages and converting power to the stable, grid-compliant AC form required for widespread use. As the demand for green energy grows, so does the need for high-performance, high-gain power conversion topologies.

However, power converters are not simple static devices; they are complex, switched-mode systems whose behavior is determined by the high-frequency switching of semiconductor devices. To ensure proper, safe, and efficient operation—such as maintaining a constant output voltage despite variations in the input source or the load—a sophisticated closed-loop control system is indispensable. This controller continuously monitors the converter's variables and adjusts the switching pattern in real-time to regulate its behavior and ensure stability under all operating conditions (ERICKSON; MAKSIMOVIĆ, 2020).

The design of an effective and robust control system is critically dependent on a thorough understanding of the converter's dynamic behavior. This is where mathematical modeling becomes an essential, preliminary step in the design process. Modeling involves deriving a set of mathematical equations, typically in the form of transfer functions, that accurately describe how the converter's state variables (such as inductor currents and capacitor voltages) respond to small disturbances in control inputs or line voltage (CUK, 1976). By providing a precise representation of the converter's dynamics, this model provides the foundation upon which all subsequent control design, analysis, and optimization are built.

The main objective of this work is to establish a generalized modeling methodology for DC-DC converters that employ the Four-State Switching Cell with a Wide Conversion Range (WCR-4SSC). By applying the state-space averaging technique, this research derives the set of small-signal transfer functions that describe the converter's dynamics in continuous conduction mode (CCM). This work is organized into six chapters:

- Chapter 2 presents a literature review of existing modeling techniques for similar converters and establishes the motivation and contributions of this research.
- Chapter 3 provides a detailed analysis of the WCR-4SSC, explaining its fundamental operating principles and deriving its governing equations across various switching stages.
- Chapter 4 describes the theoretical framework of the state-space averaging technique, the primary mathematical tool used in this work, and demonstrates the practical application of the methodology by developing the linearized averaged model for the WCR-4SSC Ćuk converter, from which its key small-signal transfer functions are derived.
- Chapter 5 validates the derived analytical model by comparing its predicted behavior against simulation results, covering both frequency-domain analysis (Bode plots) and time-domain transient responses.
- Chapter 6 summarizes the main conclusions and key contributions of the work and proposes directions for future research

Finally, the Appendices consolidate essential supplementary materials. This includes the MATLAB codes developed for analysis (Appendix A), the complete set of derived transfer function coefficients for other classical topologies, which serve to further validate the generalized nature of the proposed methodology (Appendix B), and the PSIM simulation schematic (Appendix C).

2 LITERATURE REVIEW AND MOTIVATION OF THIS WORK

The global trend of producing green energy has demanded the development of power converters capable of processing high power and stepping up low voltages from different renewable sources, like photovoltaic panels and wind turbines. The use of multiphase converters is one solution, as it permits current sharing between semiconductors, allowing for high-power processing. Furthermore, the high-frequency ripple—which is several times greater than the switching frequency—reduces the volume of the filter elements, thereby increasing the solution's power density. Within this context, a prominent family of topologies based on the three-state switching cell (3SSC) and the multistate switching cell (MSSC) has emerged as an effective solution, forming the foundation of the converters analyzed in this work.

This section provides a historical overview of the development of the WCR-4SSC and reviews the key modeling techniques applied to this family of converters.

2.1 Origin of the WCR-4SSC

A family of multiphase converters based on the 3SSC was first proposed in (BASCOPE; BARBI, 2000) and later extended for the four-state cell (4SSC) in (PERACA; BARBI, 2005). Figure 1 shows each cell. Although high power can be achieved with these topologies, in CCM the voltage gain is the same as the classical converters.

Figure 1 – Basic switching cells for the conception of interleaved converters: (a) Three-State Switching Cell, (b) Four-State Switching Cell

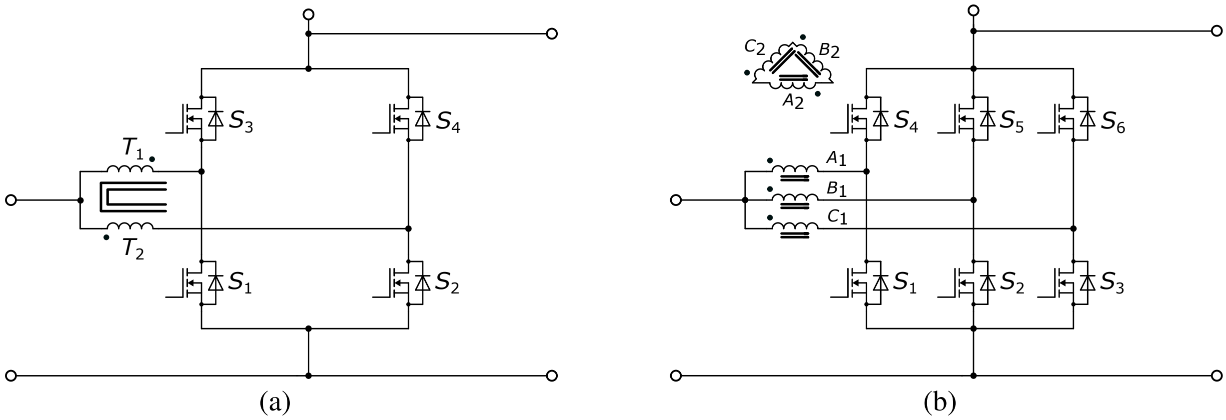

(a) (b)

Source: Adapted from (BASCOPE; BARBI, 2000) and (PERACA; BARBI, 2005)

To overcome this issue, strategies for obtaining high-step-up topologies were developed. The use of extra windings and a voltage doubler was explored in (TORRICO-BASCOPE *et al.*, 2006) and (ARAUJO *et al.*, 2010) for the 3SSC, as presented in Figure 2, where *N* represents the turns-ratio.

Figure 2 – The 3SSC cell with transformer and voltage doubler

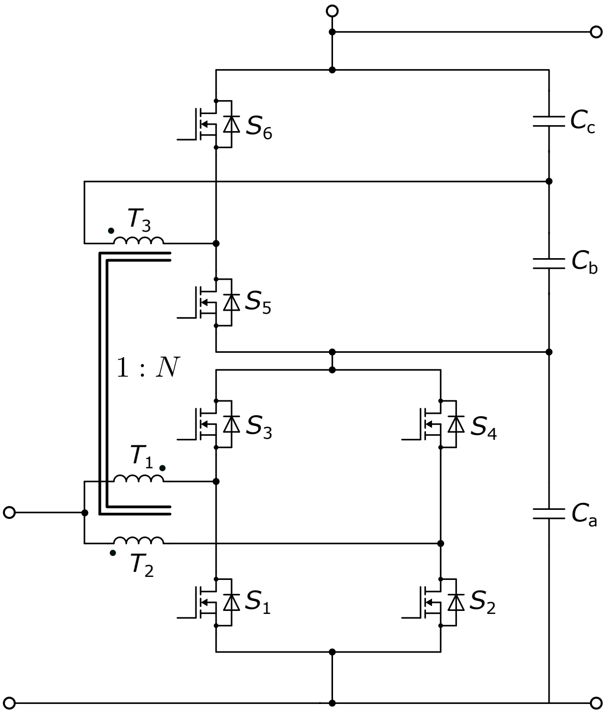

Source: Adapted from (ARAUJO *et al.*, 2010)

Finally, the use of a multi-phase transformer together with the MSSC was presented in (TORRICO-BASCOPé *et al.*, 2011). When a three-phase transformer is used, we have the so-called **Four**-**S**tate **S**witching **C**ell with a **W**ide **C**onversion **R**ange (**WCR-4SSC**), shown in Figure 3.

The WCR-4SSC integrates the well-established benefits of multiphase converters with the high voltage gain achieved through multiple secondary windings. In (BASTOS *et al.*, 2020), a family of non-isolated high-gain converters was derived by replacing the conventional canonical cell in classical topologies.

Figure 3 – The WCR-4SSC

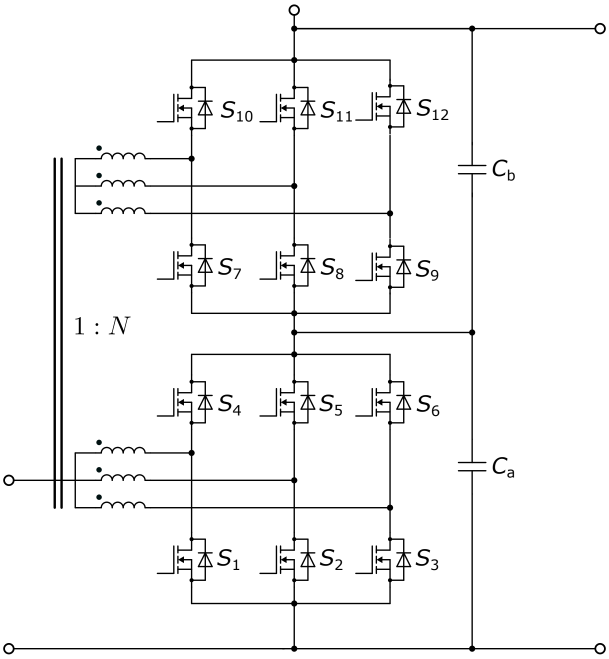

Source: Adapted from (BASTOS *et al.*, 2020).

2.2 Modeling and small-signal models

This section reviews foundational studies on the modeling of multi-state switching cell, highlighting the primary contributions and key results that motivate the present work.

In (MACIEL *et al.*, 2018), a unified small-signal model for converters based on the 3SSC operating in CCM was presented. The authors employed an approach analogous to the Pulse Width Modulation (PWM) switch model—a technique noted for its circuit-oriented simplicity. This methodology results in the generalized AC equivalent circuit shown in Figure 4.

Figure 4 – Ac model used to represent 3SSC-based dc-dc converters in CCM.

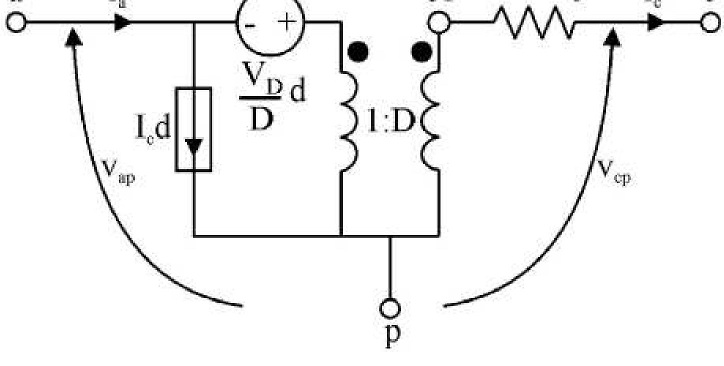

Source: (MACIEL *et al.*, 2018).

The model's validity was then demonstrated on a 3SSC buck converter through a robust validation process. This included comparing the analytical Bode plots against simulation results. A key finding is that the derived transfer functions for the 3SSC-based converter are identical to those of a conventional buck converter.

The study of the 4SSC in discontinuous conduction mode (DCM) was addressed in (TOFOLI, 2024b). Similar to the previously reviewed work on the 3SSC, the author uses a methodology analogous to the PWM switch model. The resulting generic AC model is shown below.

Figure 5 – AC model of the PWM switch representing 4SSC-based converters operating in DCM.

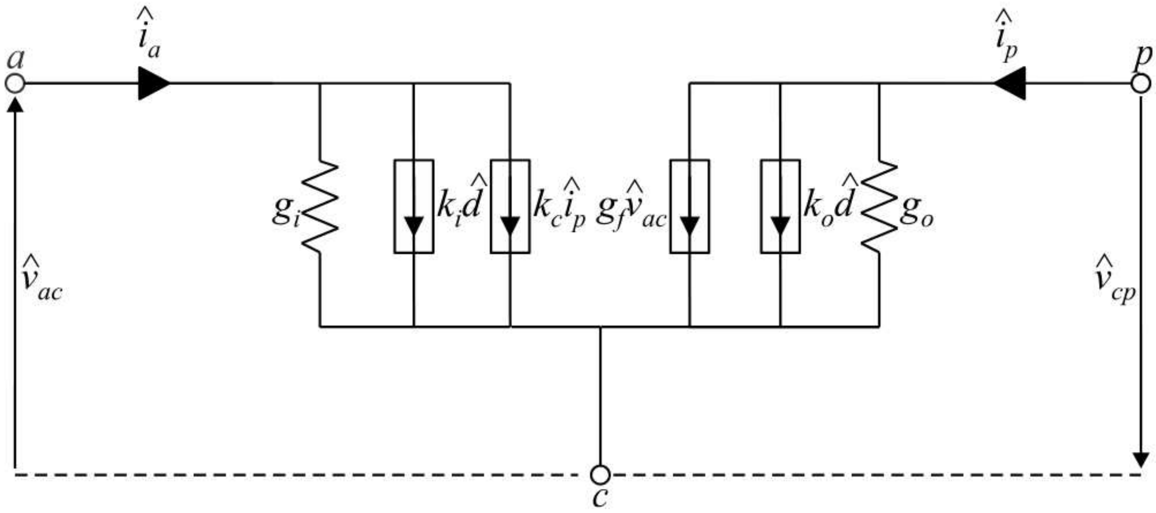

Source: (TOFOLI, 2024b).

Although the structure is the same, the paper derives the unique set of coefficients for the model’s parameters (e.g., k_i, k_c, k_o, g_i, g_f, and g_o) for each specific region (R1, R2, and R3), depending upon the steady-state duty-cycle. The derived models are thoroughly validated by applying them to a 4SSC-based buck converter. The paper shows excellent agreement between the analytical model’s predictions and simulation results

This research was later generalized for the MSSC operating in DCM in (TOFOLI, 2024a). In this work, the same PWM switch model shown in Figure 5 is used. However, its coefficients are derived as generic functions of the number of phases (M) and the specific operating region. This makes the methodology universally applicable to any MSSC topology, including the 2SSC, 3SSC, 4SSC, and even theoretical converters such as a 5SSC.

The paper validates its generalized equations through demonstration that by substituting the appropriate values for M (e.g., M=2 for 2SSC, M=3 for 3SSC), the generic formulas simplify to match the specific results derived in previous, dedicated studies. It further showcases the model’s applicability by analyzing a complete control system for a theoretical 5SSC-based buck converter.

The literature review thus far has covered modeling approaches for converters based on the 3SSC, 4SSC, and the generalized MSSC. However, the dynamic analysis of converters incorporating the WCR-4SSC was first explored in (HONORIO *et al.*, 2023). This foundational work on WCR converters introduces an equivalent converter approach to model the WCR-4SSC Boost converter. The technique aims to simplify the complex, multiphase topology by representing it as a classic, single-switch boost converter, as shown in Figure 6.

Figure 6 – Equivalent circuit approach to modeling WCR-4SSC converters: (a) WCR-4SSC DC-DC Boost converter, (b) Equivalent boost converter

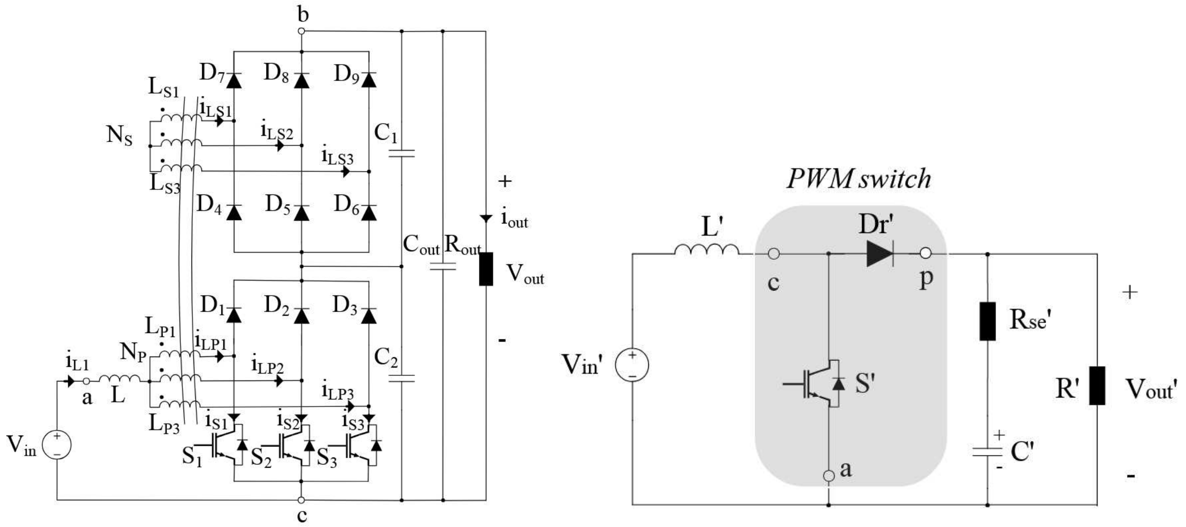

(a) (b)

Source: (HONORIO *et al.*, 2023)

Once the equivalent converter is defined, the authors apply the well-known PWM switch model to it to obtain its transfer functions. The validity of this simplification is then tested by comparing the Bode plots of the analytical model (from the equivalent converter) against two different simulation methods performed on the full WCR-4SSC circuit: an automated AC sweep and a manual point-by-point frequency response analysis.

A notable contribution is the presentation of a physical test workbench, including a prototype of the WCR-4SSC Boost converter, built to enable future experimental validation of the proposed models and control strategies.

Although the equivalent converter approach offers a practical simplification for control design, it has significant limitations. A key issue is the model’s accuracy, as notable discrepancies appear between the analytical and simulated Bode plots, particularly in the phase response at higher frequencies. The primary drawback, however, is the method's lack of generalizability. The equivalency is specifically derived for the WCR-4SSC Boost converter operating within a narrow range (Region 2). Applying this type of methodology to different operating regions, converter topologies, or with modified parameters (such as the transformer turns-ratio) can lead to incorrect conclusions.

While the equivalent converter method offers a practical shortcut, its limitations highlight the need for a more fundamental and robust modeling technique. Therefore, the primary motivation of this work is to develop such a methodology. By using the rigorous state-space averaging technique , this research aims to derive a universally applicable model for WCR-4SSC converters operating in CCM. The goal is to create a model that can be reliably extended to different topologies, parameter variations, and operating regions, thereby providing a solid foundation for understanding the dynamic behavior of these converters and for effective control design.

3 THE FOUR-STATE SWITCHING CELL WITH WIDE-CONVERSION RANGE

This chapter begins by examining the three-phase transformer, deriving key voltage and current relationships based on its physical structure and magnetic properties. Subsequently, the switching operation of the cell in continuous conduction mode is analyzed. This involves exploring the different circuit configurations that arise across its three distinct operating regions (R1, R2, and R3) to ultimately establish the terminal characteristics relating the cell's input and output variables (v_1, i_1, v_2, i_2).

3.1 Study of the transformer

To accurately model the switching cell shown in Figure 3, it is essential to analyze the operation of the three-phase transformer. Figure 7 illustrates a physical implementation of the transformer. The following assumptions are considered:

- Turns ratio equals $N = n_2/n_1$
- The self-inductance of all the primary windings are equal $(L_{A1} = L_{B1} = L_{C1} = L_P)$
- The self-inductance of all the secondary windings are equal $(L_{A2} = L_{B2} = L_{C2} = L_S = N^2 L_P)$
- The magnetic core is symmetric
- The resistance of the windings is considered negligible

Figure 7 – Physical structure of the transformer.

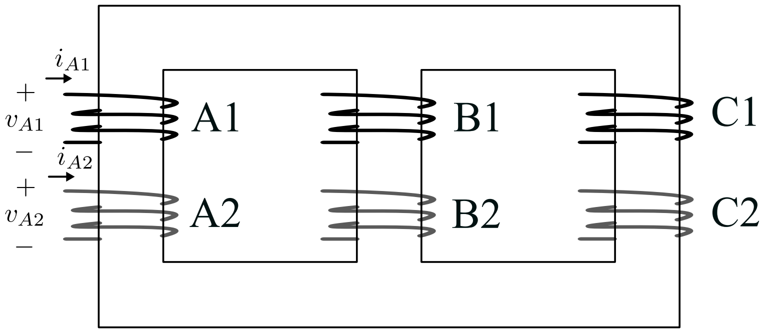

Source: The author.

The voltage across each winding is influenced by the flux linkage generated by other windings, as determined by the mutual inductance M between them. Table 1 presents the mutual inductances for different winding configurations, including two primary windings (M_{X1Y1}), a primary and a secondary winding located on the same or different core legs $(M_{X1X2}$ and M_{X1Y2}, respectively), and two secondary windings (M_{X2Y2}).

Table 1 – Mutual Inductances in a three-phase transformer.

Mutual inductance	**Value**
M_{X1Y1}	$-\frac{1}{2}L_P$
M_{X1X2}	NL_P
M_{X1Y2}	$-\frac{1}{2}NL_P$
M_{X2Y2}	$-\frac{1}{2}N^2L_P$

Source: The author.

Equation (3.1) represents the voltage across winding A1.

$$v_{A1} = L_P\dot{i}_{A1} - \frac{1}{2}L_P\dot{i}_{B1} - \frac{1}{2}L_P\dot{i}_{C1} + NL_P\dot{i}_{A2} - \frac{1}{2}NL_P\dot{i}_{B2} - \frac{1}{2}NL_P\dot{i}_{C2} \tag{3.1}$$

Similar expressions can be derived for the other windings. To analyze the current in each winding, consider the transformer modeled by a magnetizing inductance in parallel with an ideal transformer, as depicted in Figure 8.

Figure 8 – Model of the transformer including its magnetizing inductance.

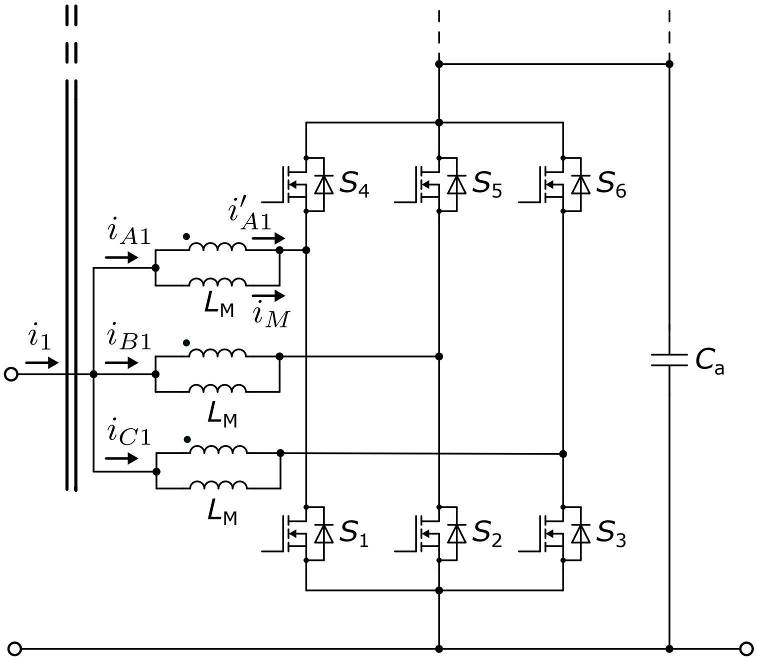

Source: The author.

Since the transformer only processes AC power, the average value over one switching period of i'_{A1} must be zero ($I'_{A1} = 0$). Consequently, $I_{A1} = I_M$, where I_M represents the DC component of the magnetizing current. Given the assumption of equal magnetizing inductances for all phases, it follows that $I_{A1} = I_{B1} = I_{C1} = I_M$. In terms of instantaneous values, the current relationship is given by:

$$i_{A1} = i_M - N i_{A2} \tag{3.2}$$

Assuming a sufficiently high magnetizing inductance, the ripple in the magnetizing current can be neglected, allowing the approximation $i_M \approx I_M$. Thus, the expression simplifies to:

$$i_{A1} = I_M - N i_{A2} \tag{3.3}$$

A similar formulation applies to the remaining windings. Equation (3.3) indicates the presence of a DC component in the primary current. Since this component is identical in all phases, the resultant DC flux has only one possible path: through the air, thereby mitigating any significant impact on core saturation. However, if the topology employs three separate single-phase transformers, each core will experience a DC flux, increasing the risk of saturation. In such cases, the transformer design must account for this effect.

3.2 The cell

The working principle of the switching cell is analyzed herein for CCM. For ease of reference, the cell is presented again in Figure 9. The control signals of the three primary low-side switches (S1, S2, and S3) are phase-shifted by 120° from each other. The corresponding high-side switches (S4, S5, and S6) operate in a complementary manner. This entire switching pattern is duplicated on the secondary side: the secondary low-side switches (S7, S8, S9) and high-side switches (S10, S11, S12) follow the same control signals as their primary counterparts.

Figure 9 – The WCR-4SSC cell

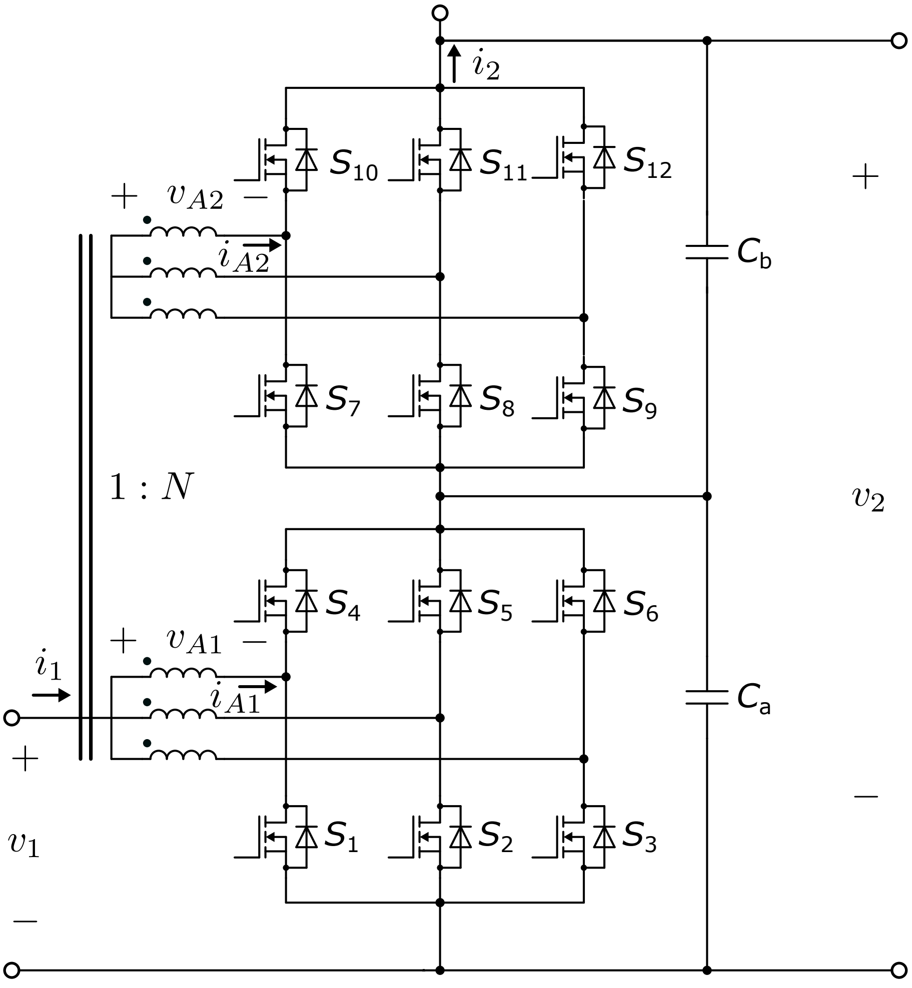

Source: Adapted from (BASTOS *et al.*, 2020).

Depending on the value of the duty cycle d, the system can operate in three distinct regions: R1 ($0 < d < 1/3$), R2 ($1/3 < d < 2/3$) and R3 ($2/3 < d < 1$). The key distinction between them is the maximum number of low-side switches that are allowed to be ON at the same time. This directly impacts how the circuit is configured at any given moment and, consequently, how it processes and transfers energy (TORRICO-BASCOPé *et al.*, 2011). The following analysis will examine the specific circuit states that arise from this switching behavior and derive the equations that govern the converter's operation, establishing the terminal characteristics of the switching cell by relating its terminal variables (v_1, i_1, v_2, i_2).

3.2.1 Region 1

In this operating region, only one low-side switch conducts at any given time, resulting in the voltage waveforms shown in Figure 10.

Figure 10 – Voltage waveforms in Region 1

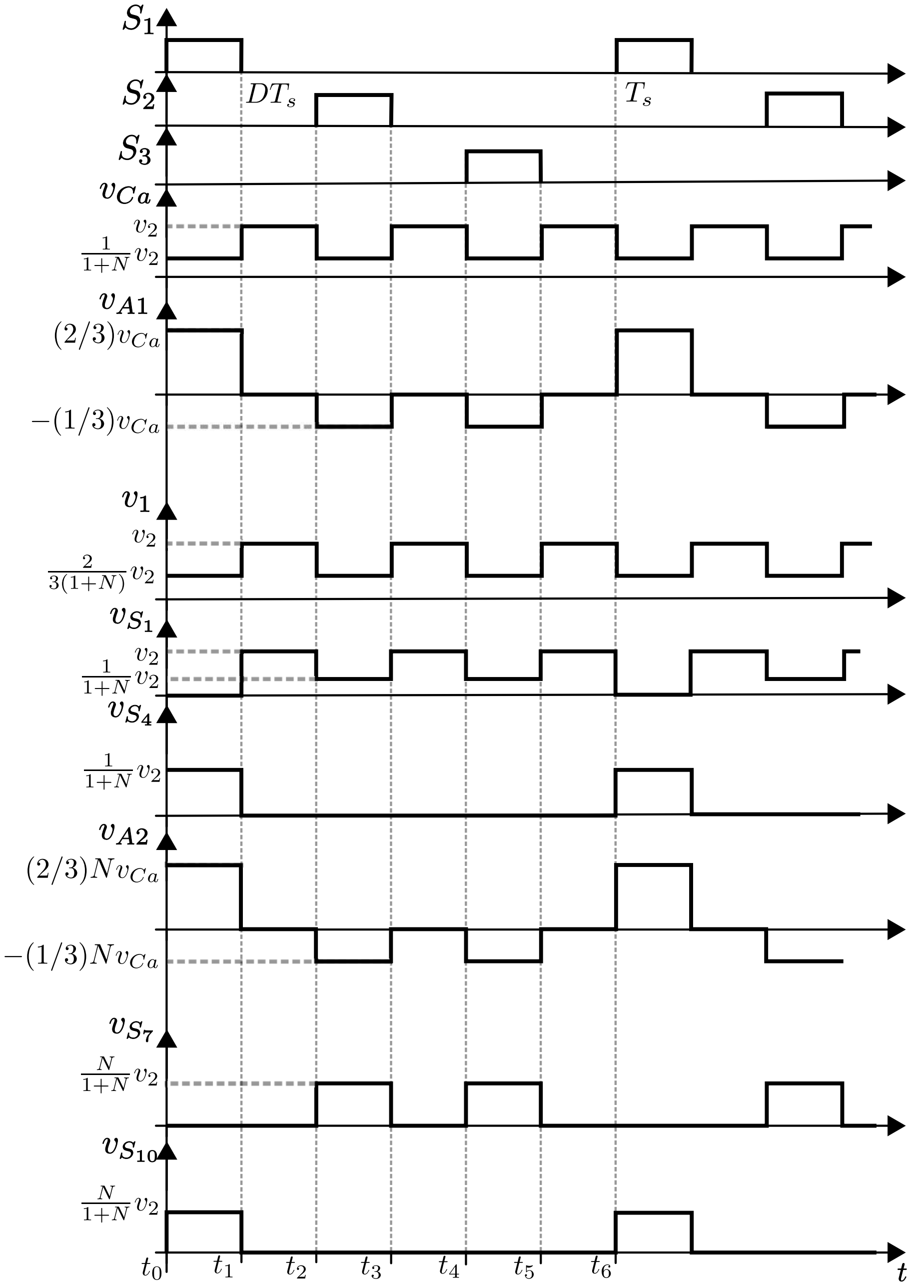

Source: The author.

3.2.1.1 1st Stage

The first stage of operation occurs during the interval $t_0 \leq t < t_1$, when switch S1 is ON. The corresponding equivalent circuit for this stage is depicted in Figure 11.

Figure 11 – Equivalent circuit when S1 is conducting

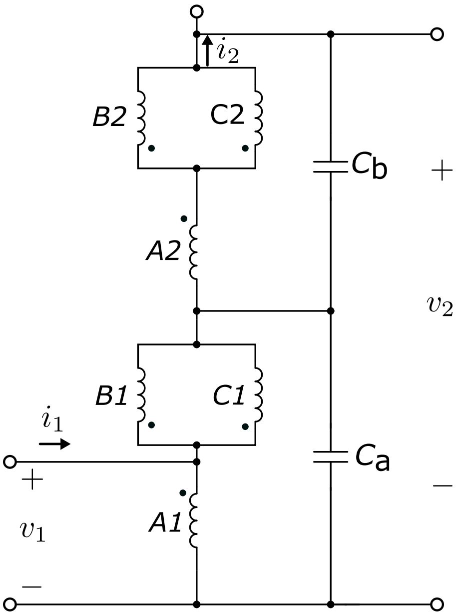

Source: The author.

From the loop formed by windings B1 and C1, one obtains:

$$v_{B1} - v_{C1} = 0 \tag{3.4}$$

Rewriting the above equation in terms of mutual inductances and the currents through the various transformer windings, as we did in Equation (3.1), results in:

$$\begin{aligned} L_P\left(\dot{i}_{B1} - \frac{\dot{i}_{A1}}{2} - \frac{\dot{i}_{C1}}{2}\right) + NL_P\left(\dot{i}_{B2} - \frac{\dot{i}_{A2}}{2} - \frac{\dot{i}_{C2}}{2}\right) - L_P\left(\dot{i}_{C1} - \frac{\dot{i}_{A1}}{2} - \frac{\dot{i}_{B1}}{2}\right) \\ + NL_P\left(\dot{i}_{C2} - \frac{\dot{i}_{A2}}{2} - \frac{\dot{i}_{B2}}{2}\right) = 0 \end{aligned} \tag{3.5}$$

Simplification leads to:

$$(\dot{i}_{B1} - \dot{i}_{C1}) + N(\dot{i}_{B2} - \dot{i}_{C2}) = 0 \tag{3.6}$$

From the loop composed of windings A1 and B1 through capacitor C_a, one obtains:

$$v_{Ca} + v_{B1} - v_{A1} = 0 \tag{3.7}$$

Rewriting and simplifying the above equation results in:

$$\frac{2}{3L_P}v_{Ca} + (\dot{i}_{B1} - \dot{i}_{A1}) + N(\dot{i}_{B2} - \dot{i}_{A2}) = 0 \tag{3.8}$$

Summing Equations (3.6) and (3.8) and rearranging terms results in:

$$v_{A1} = \frac{2}{3}v_{Ca} \tag{3.9}$$

From this result, Equation (3.10) is derived:

$$v_2 = \frac{3(1+N)}{2} \cdot v_1 \tag{3.10}$$

For the current analysis, capacitors C_a and C_b are disregarded, as in a practical design their capacitance is significantly low, making their contribution to the current analysis negligible. The currents in the secondary windings are determined as:

$$i_{A2} = -i_2 \tag{3.11}$$

$$i_{B2} = \frac{1}{2}i_2 \tag{3.12}$$

$$i_{C2} = \frac{1}{2}i_2 \tag{3.13}$$

The current in the primary windings can be obtained from (3.3).

$$i_{A1} = I_M + Ni_2 \tag{3.14}$$

$$i_{B1} = I_M - N\frac{1}{2}i_2 \tag{3.15}$$

$$i_{C1} = I_M - N\frac{1}{2}i_2 \tag{3.16}$$

From Kirchoff's current law, summing all primary currents must result in i_1. Therefore:

$$I_M = \frac{1}{3}i_1 \tag{3.17}$$

From Figure 11, it can be observed that $i_{B1} = i_{B2}$. Consequently, by using Equations (3.12), (3.15), and (3.17), the following expression is obtained:

$$i_2 = \frac{2}{3(1+N)} \cdot i_1 \tag{3.18}$$

The relationships between the terminal variables, as defined in Equations (3.10) and (3.18), remain the same regardless of which low-side switch is conducting. The same results are obtained whether S1, S2, or S3 is the active switch.

3.2.1.2 2nd Stage

The second stage of operation occurs during the interval $t_1 \leq t < t_2$, when none of the low-side switches is conducting. The corresponding equivalent circuit for this stage is depicted in Figure 12.

Figure 12 – Equivalent circuit when all low-side switches are open

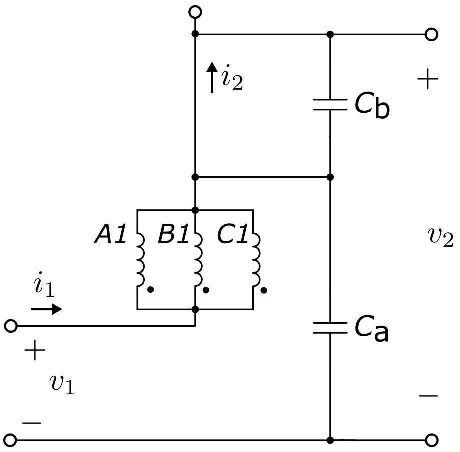

Source: The author.

The current flows through the primary and secondary high-side switches, as well as through the body diodes of switches S7 to S9. We can derive that:

$$v_{A1} = v_{B1} = v_{C1} \tag{3.19}$$

Following the same procedure used to derive (3.1), we can express Equation (3.19) in terms of the winding currents and mutual inductances. After some algebraic manipulation, this yields:

$$v_2 = v_1 \tag{3.20}$$

$$i_2 = i_1 \tag{3.21}$$

3.2.1.3 3rd-6th Stage

The remaining stages of operation occur during the interval $t_2 \leq t < t_6$. The 3^{rd} and 5^{th} stages exhibit similarity to the 1^{st} stage, as both involve the activation of a single low-side switch. Consequently, Equations (3.10) and (3.18) remain applicable. The equivalent circuit depicted in Figure 11 is still valid, with the only distinction being the winding order. Similarly, the 4^{th} and 6^{th} stages are similar to the 2^{nd} stage, as they do not involve the activation of any low-side switches. Thus, the equivalent circuit illustrated in Figure 12 and Equations (3.20) and (3.21) remain valid.

3.2.1.4 *Equivalent Two-Stage Model*

Although the converter cycles through six distinct operational stages, its terminal behavior can be simplified into just two equivalent stages. This allows us to conceptualize an equivalent switch, S^*, governed by an equivalent duty cycle, d^*, which operates at three times the converter's switching frequency ($T_s^* = 1/3 \cdot T_s$), as illustrated in Figure 13.

Figure 13 – Equivalent duty-cycle d^* and switching period T_s^* for Region 1

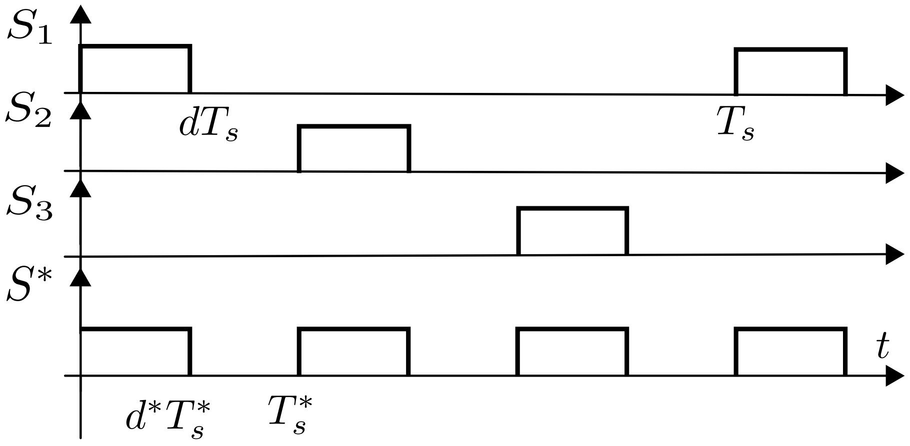

Source: The author.

This simplified two-stage representation forms the basis for applying the state-space averaging technique. Through simple waveform analysis, the relationship between the equivalent duty cycle (d^*) and the actual duty cycle (d) is found to be:

$$d^* = 3d \tag{3.22}$$

3.2.2 Region 2

In this operating region, one or two low-side switches conduct at any given time, resulting in the voltage waveforms shown in Figure 14.

Figure 14 – Voltage waveforms in Region 2

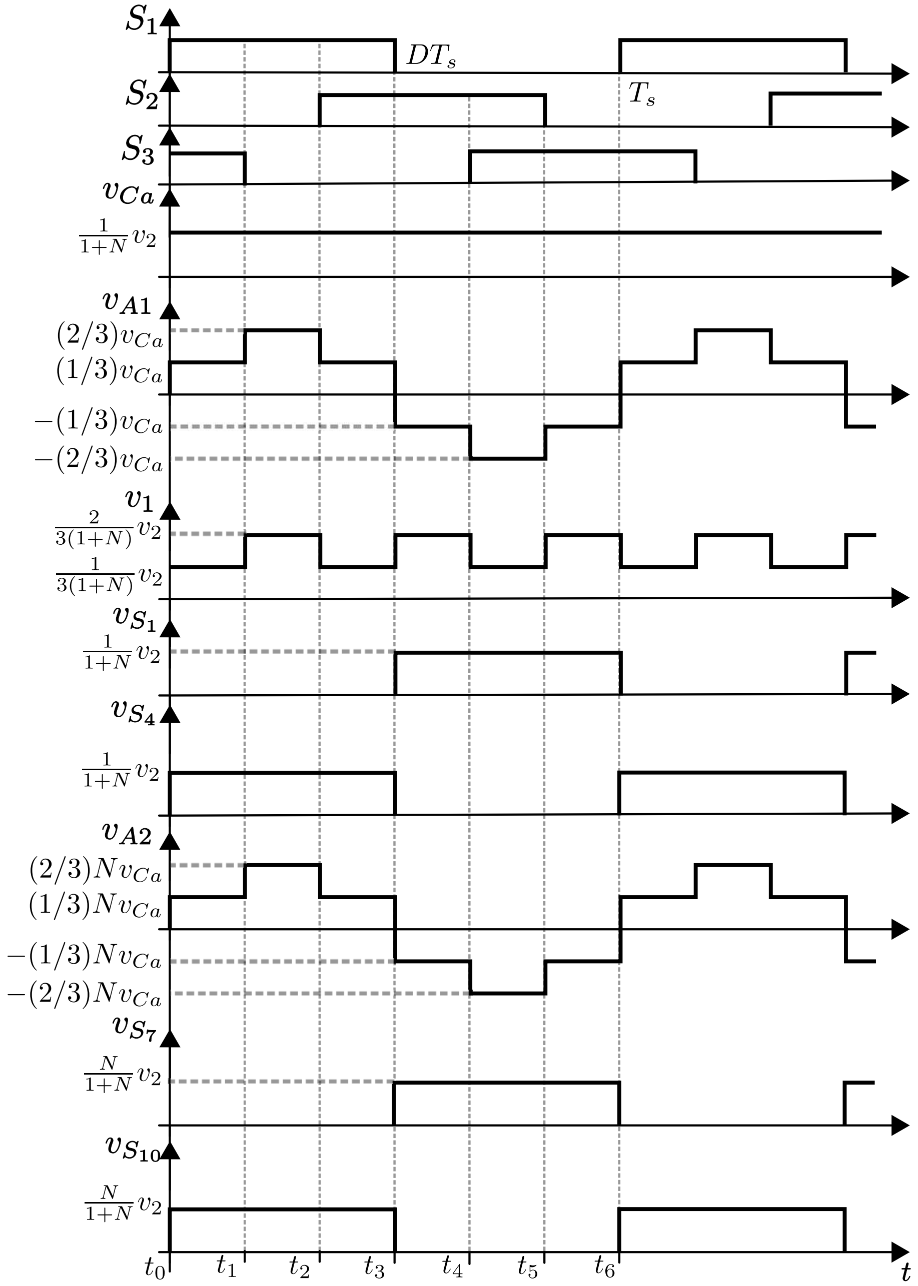

Source: The author.

3.2.2.1 1st Stage

The first stage of operation occurs during the interval $t_0 \leq t < t_1$, when switches S1 and S3 are conducting. The corresponding equivalent circuit for this stage is depicted in Figure 15.

Figure 15 – Equivalent circuit when S1 and S3 are conducting

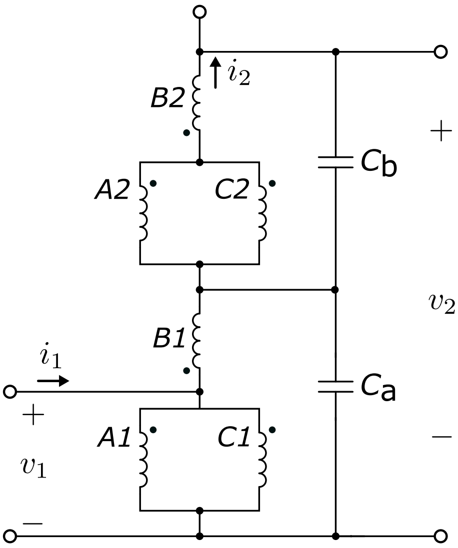

Source: The author.

From the loop formed by windings A1 and C1, one obtains:

$$v_{A1} - v_{C1} = 0 \tag{3.23}$$

From the loop composed of windings B1 and C1 through capacitor C_a, one obtains:

$$v_{Ca} + v_{B1} - v_{C1} = 0 \tag{3.24}$$

Following a similar procedure developed in Region 1, these results are obtained:

$$v_2 = 3(1+N) \cdot v_1 \tag{3.25}$$

$$i_2 = \frac{1}{3(1+N)} \cdot i_1 \tag{3.26}$$

The same result is obtained if any other combination of two low-side switches is considered to be ON.

3.2.2.2 2nd Stage

The second stage of operation occurs during the interval $t_1 \leq t < t_2$, when only switch S1 is conducting. The corresponding equivalent circuit for this stage is the same as shown in Figure 11. Therefore, Equations (3.10) and (3.18) are valid.

3.2.2.3 3rd-6th Stage

The 3^{rd} and 5^{th} stages exhibit similarity to the 1^{st} stage. Consequently, Equations (3.25) and (3.26) remain applicable. The equivalent circuit depicted in Figure 15 is still valid, with the only distinction being the winding order. Similarly, the 4^{th} and 6^{th} stages are similar to the 2^{nd} stage. Thus, the equivalent circuit illustrated in Figure 11 and Equations (3.10) and (3.18) remain valid.

3.2.2.4 Equivalent Two-Stage Model

Although the converter cycles through six distinct operational stages, its terminal behavior can be simplified into just two equivalent stages. This allows us to conceptualize an equivalent switch, S^*, governed by an equivalent duty cycle, d^*, which operates at three times the converter's switching frequency ($T_s^* = 1/3 \cdot T_s$), as illustrated in Figure 16.

Figure 16 – Equivalent duty-cycle d^* and switching period T_s^* for Region 2

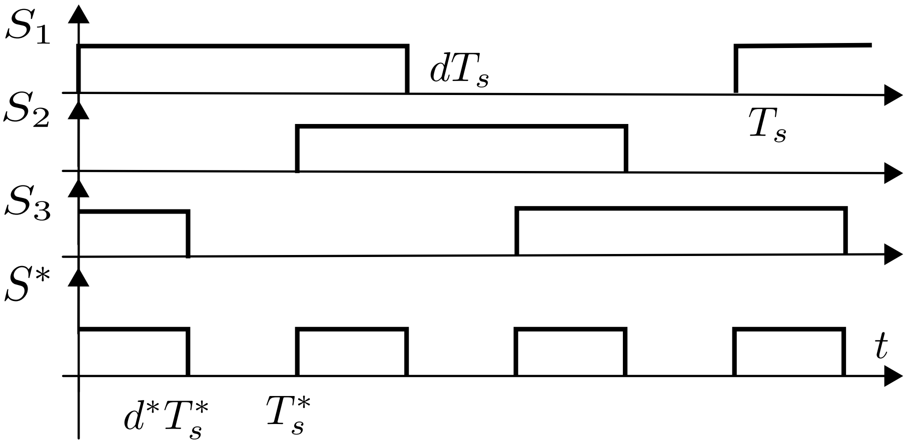

Source: The author.

Through simple waveform analysis, the relationship between the equivalent duty cycle (d^*) and the actual duty cycle (d) is found to be:

$$d^* = 3d - 1 \tag{3.27}$$

3.2.3 Region 3

In this operating region, two or three low-side switches conduct at any given time, resulting in the voltage waveforms shown in Figure 17.

Figure 17 – Voltage waveforms in Region 3

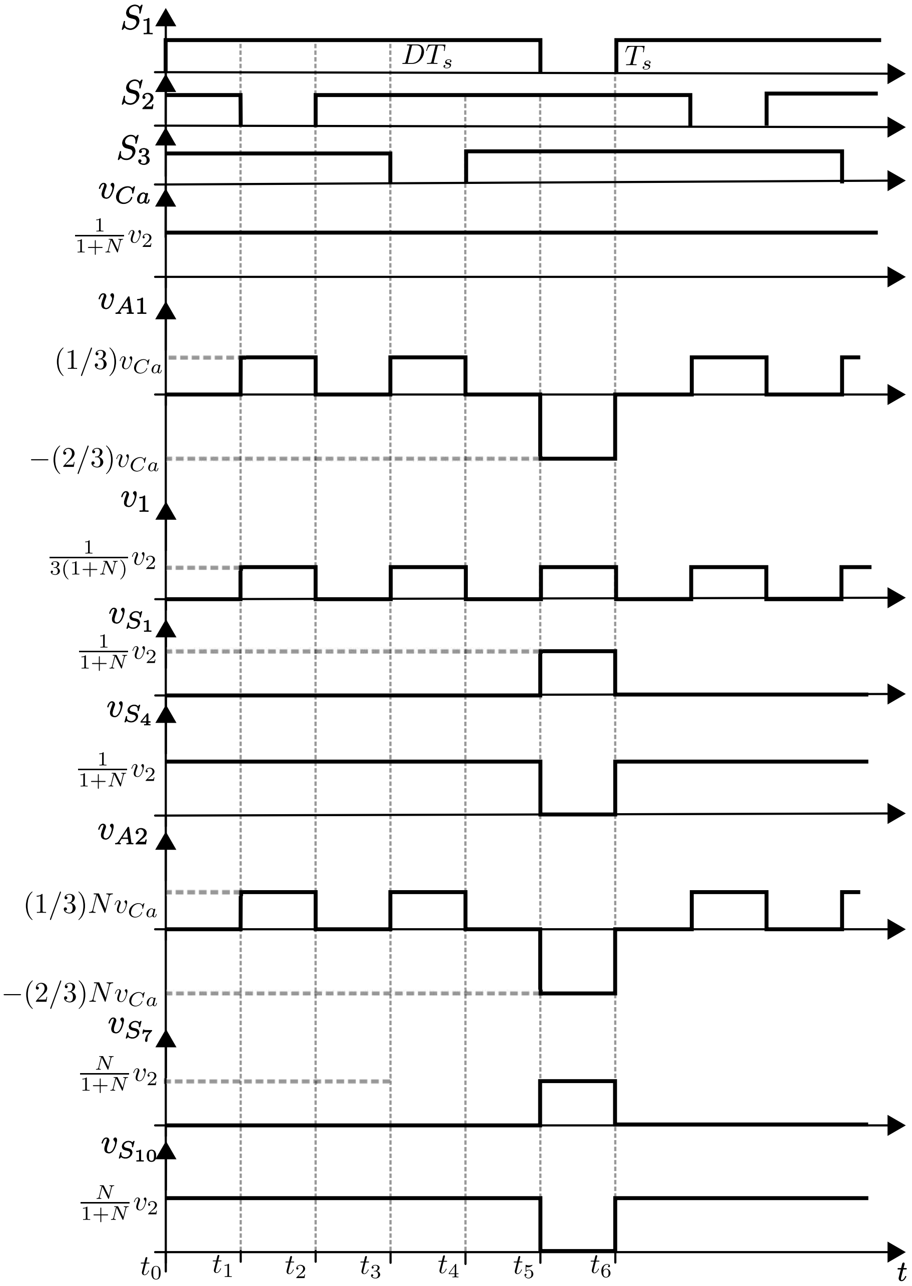

Source: The author.

3.2.3.1 1st Stage

The first stage of operation occurs during the interval $t_0 \leq t < t_1$, when switches S1, S2, and S3 are conducting. The corresponding equivalent circuit for this stage is depicted in Figure 18.

Figure 18 – Equivalent circuit when S1, S2, and S3 are conducting

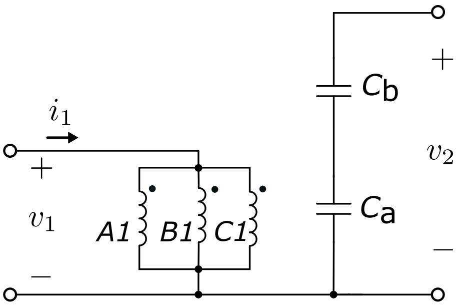

Source: The author.

From the circuit, it is possible to write the following equality:

$$v_{A1} = v_{B1} = v_{C1} = 0 \tag{3.28}$$

Therefore:

$$v_1 = 0 \tag{3.29}$$

$$i_2 = 0 \tag{3.30}$$

3.2.3.2 2nd Stage

The second stage of operation occurs during the interval $t_1 \leq t < t_2$, when only switch S1 and S3 are conducting. The corresponding equivalent circuit for this stage is the same as shown in Figure 15. Therefore, Equations (3.25) and (3.26) are valid.

3.2.3.3 3rd-6th Stage

The remaining stages of operation occur during the interval $t_2 \leq t < t_6$. The 3^{rd} and 5^{th} stages exhibit similarity to the 1^{st} stage, as both involve the activation of all low-side switches. Consequently, Equations (3.29) and (3.30) remain applicable. The equivalent circuit depicted in Figure 18 is still valid. Similarly, the 4^{th} and 6^{th} stages are similar to the 2^{nd} stage, as they involve the activation of two low-side switches. Thus, the equivalent circuit illustrated in Figure 15 and Equations (3.25) and (3.26) remain valid.

3.2.3.4 Equivalent Two-Stage Model

The converter's six-stage operation can be simplified into a two-stage equivalent model. This allows us to conceptualize an equivalent switch, S^*, governed by an equivalent duty cycle, d^*, which operates at three times the converter's switching frequency ($T_s^* = {}^1\!/_3 \cdot T_s$), as illustrated in Figure 19.

Figure 19 – Equivalent duty-cycle d^* and switching period T_s^* for Region 3

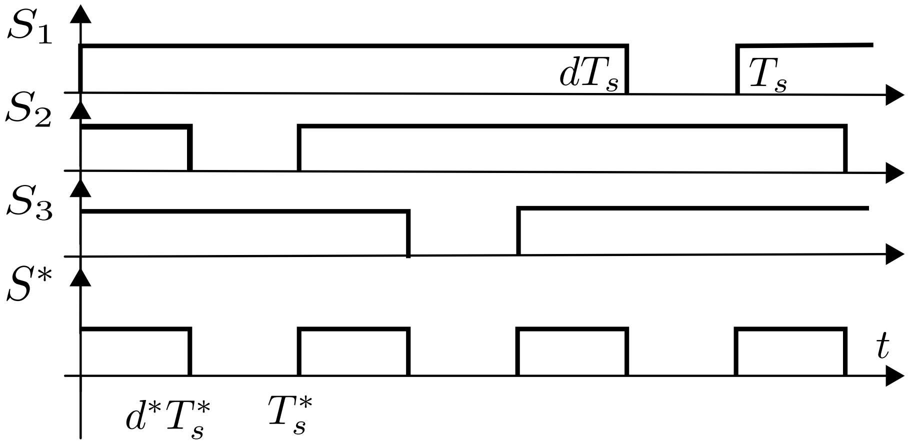

Source: The author.

Through simple waveform analysis, the relationship between the equivalent duty cycle (d^*) and the actual duty cycle (d) is found to be:

$$d^* = 3d - 2 \tag{3.31}$$

3.3 Summary

This subsection summarizes the key findings derived throughout this chapter regarding the terminal characteristics of the WCR-4SSC. As demonstrated, the relationships between the cell variables differ depending on the operating region (R1, R2, or R3) and the specific equivalent stage within that region. Table 2 consolidates these crucial relationships and presents the corresponding formula for the equivalent duty cycle applicable to each region.

Table 2 – Summary of cell relationships and equivalent duty cycle per region.

Region	**Cell Terminal Equations**		**Equivalent Duty-Cycle**
	First Stage	**Second Stage**	
1	$v_2 = \frac{3(1+N)}{2} \cdot v_1$ $i_2 = \frac{2}{3(1+N)} \cdot i_1$	$v_2 = v_1$ $i_2 = i_1$	$d^* = 3d$
2	$v_2 = 3(1+N) \cdot v_1$ $i_2 = \frac{1}{3(1+N)} \cdot i_1$	$v_2 = \frac{3(1+N)}{2} \cdot v_1$ $i_2 = \frac{2}{3(1+N)} \cdot i_1$	$d^* = 3d - 1$
3	$v_1 = 0$ $i_2 = 0$	$v_2 = 3(1+N) \cdot v_1$ $i_2 = \frac{1}{3(1+N)} \cdot i_1$	$d^* = 3d - 2$

Source: The author.

4 PROPOSED MODELING METHODOLOGY

This chapter presents the core contribution of the work: a systematic methodology for modeling DC-DC converters that utilize the WCR-4SSC. The following sections first detail the theoretical background of the state-space averaging technique. This theory is then consolidated into a formal step-by-step procedure. Finally, to demonstrate the methodology's practical application, the WCR-4SSC Ćuk converter is analyzed as a comprehensive example.

4.1 State-space averaging technique

This chapter details the state-space averaging (SSA) technique, the mathematical methodology employed in this work to derive the dynamic model of converters utilizing the WCR-4SSC. Building upon the equivalent two-stage representation established in the previous chapter, this section explains how SSA averages the converter's behavior over a switching cycle to obtain a single, continuous model.

4.1.1 Theoretical background

In power converters, the system operates in different topological states due to the switching behavior of semiconductor devices. Instead of analyzing each switching state separately, the state-space averaging technique formulates an averaged model by weighting the system's state-space equations according to the duty cycle of the switching signals (CUK, 1976).

Mathematically, the state-space representation of a power converter in each switching state is given by:

$$\begin{aligned} \dot{x} &= A_k \cdot x + B_k \cdot v_i \\ y &= C_k \cdot x \end{aligned} \tag{4.1}$$

In the equations above, x represents the state variables (e.g., inductor currents and capacitor voltages), v_i denotes the input voltage, y is the output vector, and A_k, B_k and C_k are the state-space matrices associated with the k-th switching state.

Even though the WCR-4SSC cycles through six distinct operational stages, the dynamics of its state variables can be represented by an equivalent two-stage model. This simplified model operates with an equivalent duty cycle d^*, whose relationship to the actual duty cycle d varies depending on the converter's operating region, as previously established.

Therefore, assuming the particular case of a two-stage converter, the modeling technique involves taking the duty-cycle-weighted average of the two state-space models. The resulting averaged model is given by:

$$\begin{aligned}\dot{\bar{x}} &= (d^* \cdot A_1 + d_1^* \cdot A_2) \cdot \bar{x} + (d^* \cdot B_1 + d_1^* \cdot B_2) \cdot v_i \\ \bar{y} &= (d^* \cdot C_1 + d_1^* \cdot C_2) \cdot \bar{x}\end{aligned} \tag{4.2}$$

where $d_1^* = 1 - d^*$.

The derived averaged state-space model, comprising a set of first-order differential equations, facilitates the simulation of the converter's time-domain transient responses. The averaged state variables $\bar{x}$ can be iteratively computed at discrete time steps Δt based on their derivatives $\dot{\bar{x}}$ as defined by Equation (4.2), as will be demonstrated in subsequent chapters.

To analyze the converter's dynamics, it is necessary to examine its response to external perturbations $\hat{v}_i$ and $\hat{d}^*$ around the operating point defined by V_i and D^*, i.e., $v_i = V_i + \hat{v}_i$ and $d^* = D^* + \hat{d}^*$. These perturbations result in variations in the system's state variables and consequently in the averaged variables, $\bar{x} = X + \hat{x}$, and in the averaged output, $\bar{y} = Y + \hat{y}$. By incorporating perturbations into Equation (4.2) and neglecting the nonlinear terms, we obtain::

$$\begin{aligned}\dot{\hat{x}} &= AX + BV_i + A\hat{x} + B\hat{v}_i + [(A_1 - A_2)X + (B_1 - B_2)V_i]\,\hat{d}^* \\ Y + \hat{y} &= CX + C\hat{x} + (C_1 - C_2)X\hat{d}^*\end{aligned} \tag{4.3}$$

where $A = D^* \cdot A_1 + D_1^* \cdot A_2$, with similar definitions for B and C.

Equation (4.3) represents the linearized averaged model of the DC-DC converter operating in continuous conduction mode. This equation can be further decomposed into two parts. The first describes the steady-state operation:

$$\begin{aligned}X &= -A^{-1}BV_i \\ Y &= -CA^{-1}BV_i\end{aligned} \tag{4.4}$$

The second part describes the converter's dynamic response to perturbations:

$$\begin{aligned}\dot{\hat{x}} &= A\hat{x} + B\hat{v}_i + [(A_1 - A_2)X + (B_1 - B_2)V_i]\,\hat{d}^* \\ \hat{y} &= C\hat{x} + (C_1 - C_2)X\hat{d}^*\end{aligned} \tag{4.5}$$

By setting $\hat{d}^* = 0$ in Equation (4.5) and applying the Laplace transform, we obtain the transfer functions related to variations in the input voltage:

$$\begin{aligned}\frac{\hat{x}(s)}{\hat{v}_i(s)} &= (sI - A)^{-1}B \\ \frac{\hat{y}(s)}{\hat{v}_i(s)} &= C(sI - A)^{-1}B\end{aligned} \tag{4.6}$$

Similarly, by setting $\hat{v}_i = 0$, we derive the transfer functions related to the equivalent duty cycle:

$$\begin{aligned}\frac{\hat{x}(s)}{\hat{d}^*(s)} &= (sI-A)^{-1}\left[(A_1-A_2)X+(B_1-B_2)V_i\right] \\ \frac{\hat{y}(s)}{\hat{d}^*(s)} &= C(sI-A)^{-1}\left[(A_1-A_2)X+(B_1-B_2)V_i\right]+(C_1-C_2)X\end{aligned} \tag{4.7}$$

In a real implementation, one will have control over d, not d^*. The relationship between this variables were established for each region through Equations (3.22), (3.27) and (3.31). Using the index R to specify the operating region (R=1, 2, or 3), we obtain:

$$d^* = 3d-(R-1) \tag{4.8}$$

$$(D^*+\hat{d}^*) = 3(D+\hat{d})-(R-1) \tag{4.9}$$

$$(D^*+\hat{d}^*) = (3D-R+1)+3\hat{d} \tag{4.10}$$

$$D^* = 3D-R+1 \tag{4.11}$$

$$\hat{d}^* = 3\hat{d} \tag{4.12}$$

Substituting Equation (4.12) in Equation (4.7), one obtains:

$$\begin{aligned}\frac{\hat{x}(s)}{\hat{d}(s)} &= 3\cdot(sI-A)^{-1}\left[(A_1-A_2)X+(B_1-B_2)V_i\right] \\ \frac{\hat{y}(s)}{\hat{d}(s)} &= 3\cdot C(sI-A)^{-1}\left[(A_1-A_2)X+(B_1-B_2)V_i\right]+3\cdot(C_1-C_2)X\end{aligned} \tag{4.13}$$

Equations (4.6) and (4.13) provide all the necessary transfer functions for designing controllers for a DC-DC converter employing the WCR-4SSC operating in continuous conduction mode.

4.1.2 Step-by-step procedure

1. Derive differential equations for the converter circuit

The initial step involves deriving the differential equations that model the converter. These equations are obtained by applying fundamental circuit laws (e.g., Kirchhoff's Voltage and Current Laws) to the converter circuit. The resulting expressions may contain the cell's terminal variables (v_1, i_1, v_2, i_2).

2. Formulate the standard state-space representation by substituting cell relationships

Knowing the operating region, substitute the corresponding relationships for the cell's terminal variables into the differential equations derived previously. This process yields two distinct sets of state-space matrices (A_1, B_1, C_1 and A_2, B_2, C_2), one set representing each of the two equivalent stages.

3. Obtain the averaged state-space model.

With the state-space representations for both equivalent stages, apply the state-space averaging technique as defined in Equation (4.2). Recall that the expression relating d^* to the actual duty cycle d depends on the operating region, as shown in Equation (4.8). The result is a single, averaged state-space model. This averaged model provides a continuous representation of the converter and can be used directly for time-domain simulations to analyze transient responses.

4. Derive the transfer functions

Finally, calculate the steady-state operating point using Equation (4.4). Then, apply Equations (4.6) and (4.13) to derive the desired small-signal transfer functions.

4.2 Example: WCR-4SSC Ćuk Converter

To illustrate the proposed methodology, the WCR-4SSC Ćuk converter (Figure 20) is selected as a representative example. The state variables for this system include the currents in inductors, denoted as i_{L_1} and i_{L_2}, the voltage across the coupling capacitor v_{C_c}, and the voltage across the output capacitor v_{C_o}.

Figure 20 – WCR-4SSC Ćuk Converter

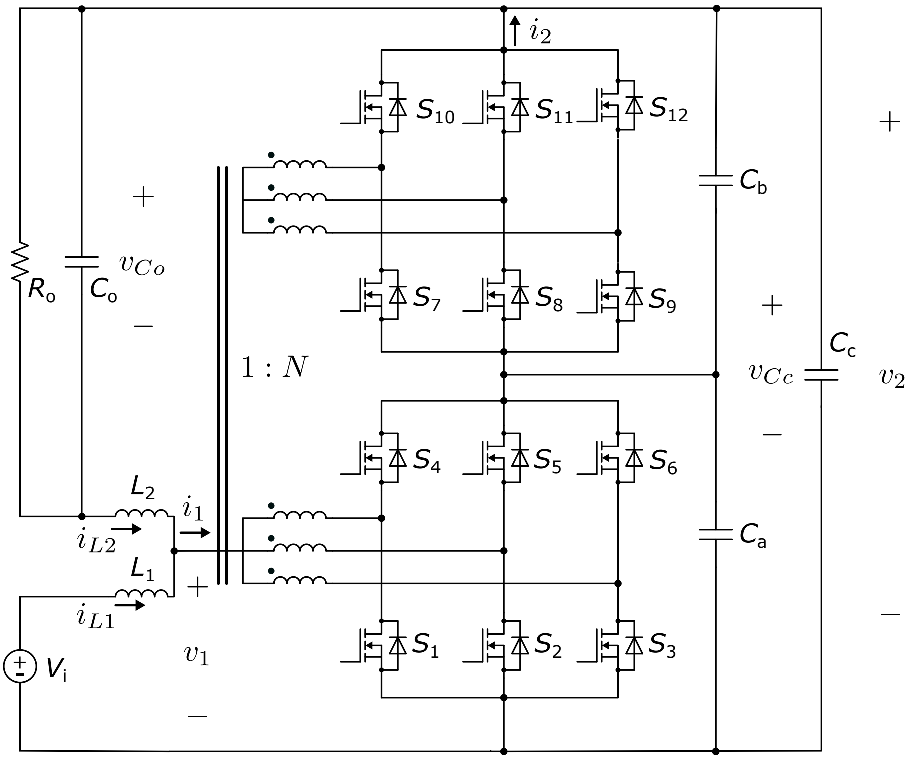

Source: Adapted from (BASTOS *et al.*, 2020).

The parameters used in this example are detailed in Table 3.

Step 1: The circuit analysis yields the following equations:

$$\dot{i}_{L_1} = -\frac{1}{L_1} \cdot v_1 + \frac{1}{L_1} \cdot V_i \tag{4.14a}$$

$$\dot{i}_{L_2} = \frac{1}{L_2} \cdot v_{C_c} - \frac{1}{L_2} \cdot v_{C_o} - \frac{1}{L_2} \cdot v_1 \tag{4.14b}$$

$$\dot{v}_{C_c} = \frac{1}{C_c} \cdot i_2 - \frac{1}{C_c} \cdot i_{L_2} \tag{4.14c}$$

$$\dot{v}_{C_o} = \frac{1}{C_o} \cdot i_{L_2} - \frac{1}{RoCo} \cdot v_{C_o} \tag{4.14d}$$

Table 3 – WCR-4SSC Ćuk converter specifications

Specification	**Notation**	**Value**	**Unit**
Input voltage	V_{in}	86	V
Output voltage	V_{in}	560	V
Switching frequency	f_s	15	kHz
Duty cycle R2	d	0.6	-
Turns ratio	N	2	-
Inductance 1	L_1	135	μH
Inductance 2	L_2	350	μH
Upper bridge capacitance	C_b	100	nF
Lower bridge capacitance	C_a	100	nF
Coupling capacitance	C_c	10	μF
Output filter capacitance	C_o	2.2	μF
Load resistance	R_o	100	Ω

Source: The author.

Step 2: To express the system equations in the standard state-space form, the cell's terminal variables v_1 and i_2 must be written in terms of the state variables and/or the input voltage. First, observe that:

$$v_2 = v_{C_c} \tag{4.15a}$$

$$i_1 = i_{L_1} + i_{L_2} \tag{4.15b}$$

Now, we incorporate the relationships for the cell's terminal variables derived in Chapter 3. These relationships depend on the specific configuration of the cell within each equivalent stage. Considering the example of operation in Region 2, the system alternates between two stages:

- First Stage: Corresponds to two low-side switches conducting. The terminal variables are related by Equations (3.25) and (3.26).
- Second Stage: Corresponds to one low-side switch conducting. The terminal variables are related by Equations (3.10) and (3.18).

Substituting these respective sets of equations into the converter's differential equations allows for the formulation of the state-space model for each stage.

Step 2.1 - First-stage: By substituting Equations (3.25) and (3.26) into Equations (4.15a) and (4.15b), one obtains:

$$v_1 = \frac{2}{3(1+N)} \cdot v_{C_c} \tag{4.16a}$$

$$i_2 = \frac{2}{3(1+N)} \cdot (i_{L_1} + i_{L_2}) \tag{4.16b}$$

Substitution of these results into Equations (4.14a)-(4.14d) and rewriting them in matrix form yields:

$$\begin{bmatrix} \dot{i}_{L_1} \\ \dot{i}_{L_2} \\ \dot{v}_{C_c} \\ \dot{v}_{C_o} \end{bmatrix} = \begin{bmatrix} 0 & 0 & -\frac{1}{L_1} \cdot \frac{1}{3(1+N)} & 0 \\ 0 & 0 & \frac{1}{L_2}\left[1 - \frac{1}{3(1+N)}\right] & -\frac{1}{L_2} \\ \frac{1}{C_c} \cdot \frac{1}{3(1+N)} & \frac{1}{C_c}\left[\frac{1}{3(1+N)} - 1\right] & 0 & 0 \\ 0 & \frac{1}{C_o} & 0 & -\frac{1}{RoCo} \end{bmatrix} \cdot \begin{bmatrix} i_{L_1} \\ i_{L_2} \\ v_{C_c} \\ v_{C_o} \end{bmatrix} + \begin{bmatrix} \frac{1}{L_1} \\ 0 \\ 0 \\ 0 \end{bmatrix} \cdot Vi \tag{4.17}$$

Step 2.2 - Second-stage: To derive the state-space representation for the second stage, the expressions relating the cell's terminal variables during this stage (given by Equations (3.10) and (3.18)) are substituted into Equations (4.15a) and (4.15b) and the results are applied in Equations (4.14a)-(4.14d):

$$\begin{bmatrix} \dot{i}_{L_1} \\ \dot{i}_{L_2} \\ \dot{v}_{C_c} \\ \dot{v}_{C_o} \end{bmatrix} = \begin{bmatrix} 0 & 0 & -\frac{1}{L_1} \cdot \frac{2}{3(1+N)} & 0 \\ 0 & 0 & \frac{1}{L_2}\left[1 - \frac{2}{3(1+N)}\right] & -\frac{1}{L_2} \\ \frac{1}{C_c} \cdot \frac{2}{3(1+N)} & \frac{1}{C_c}\left[\frac{2}{3(1+N)} - 1\right] & 0 & 0 \\ 0 & \frac{1}{C_o} & 0 & -\frac{1}{RoCo} \end{bmatrix} \cdot \begin{bmatrix} i_{L_1} \\ i_{L_2} \\ v_{C_c} \\ v_{C_o} \end{bmatrix} + \begin{bmatrix} \frac{1}{L_1} \\ 0 \\ 0 \\ 0 \end{bmatrix} \cdot Vi \tag{4.18}$$

Step 3:

Equation (4.2) is applied to derive the averaged state-space model, which enables time-domain analysis. A MATLAB implementation demonstrating this procedure with numerical values is available in Appendix A.

Step 4:

The desired transfer functions are obtained by applying Equations (4.6) and (4.13). As this derivation is complex and tedious to perform manually, a MATLAB code was developed to automate the calculation of both literal (symbolic) and numerical expressions (see Appendix A). The resulting literal transfer functions for Ćuk and all other classical converters operating in Region 2 are summarized in Appendix B.

Although this example focuses on Region 2, the modeling procedure is applicable to all operating regions. The fundamental steps remain the same; the only modification occurs in Step 2. For other regions, the specific relationships for the cell's terminal variables (which are substituted into the converter's differential equations) must be chosen according to the number of conducting low-side switches in each equivalent stage.

5 RESULTS

This chapter validates the proposed modeling methodology by comparing the analytical expressions developed in this work against results from PSIM simulations. The validation is performed in both the time domain (transient response) and the frequency domain (Bode plots). All comparisons use the converter specifications listed in Table 3, and the corresponding PSIM schematic is provided in Appendix C.

5.1 Time-domain

The time-domain validation was performed by comparing the simulation against the averaged state-space model implemented in MATLAB (see Appendix A).

Figure 21 shows the converter's start-up transient. The highlighted section illustrates the key difference between the averaged model, which neglects switching-frequency ripple, and the simulation, which includes it.

Figure 21 – Start-up transient

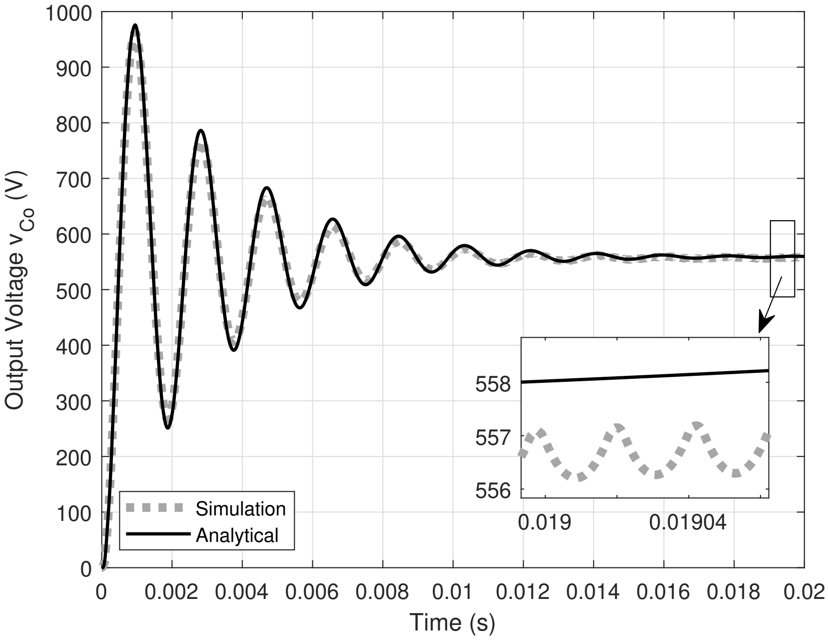

Source: The author.

At $t = 0.04\ s$, a load step was applied, changing the output resistance from 100 Ω to 200 Ω. The resulting transient response is shown in Figure 22.

Figure 22 – Load step

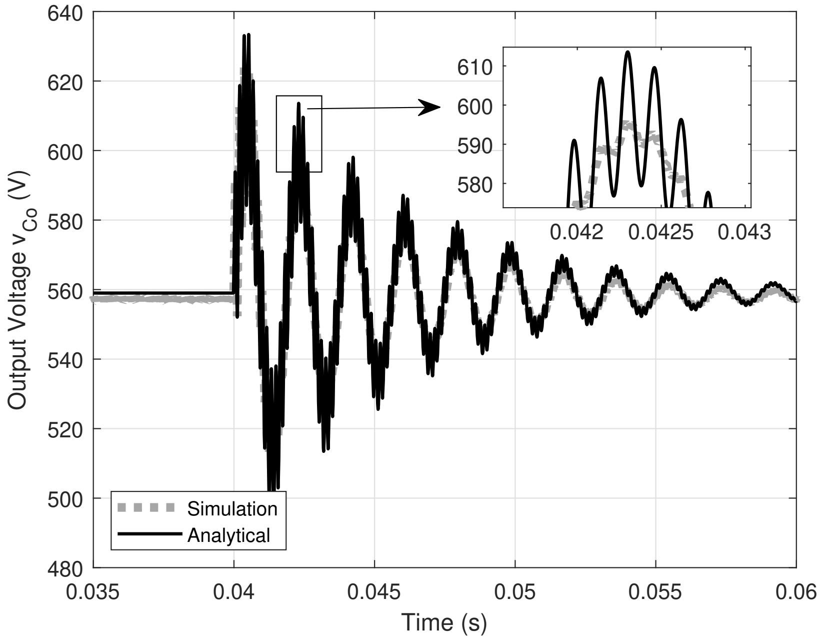

Source: The author.

At $t = 0.08\ s$, an input voltage step was applied, decreasing the voltage from 86 V to 70 V. The resulting response is shown in Figure 23.

Figure 23 – Input voltage step

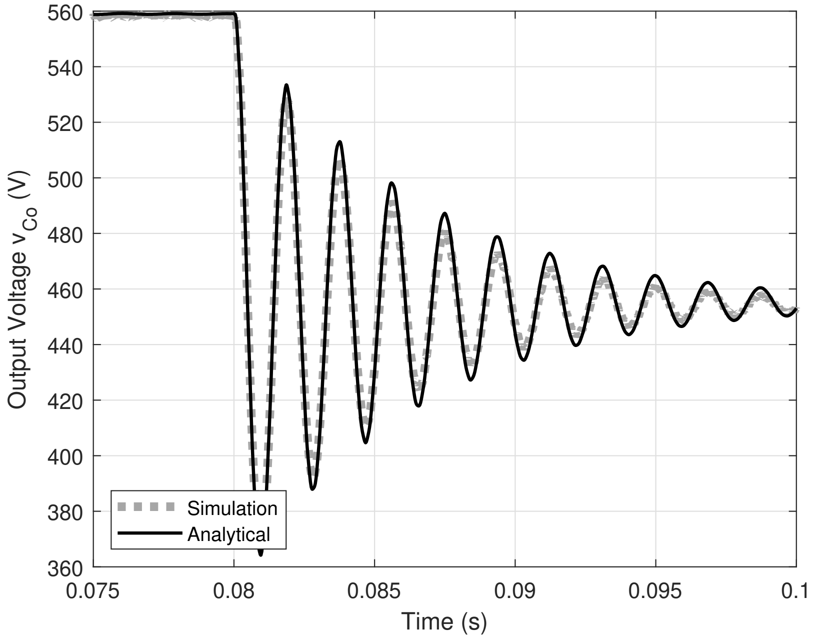

Source: The author.

Finally, at $t = 1.40\ s$, a step change in the duty cycle was applied, decreasing its value from 0.6 to 0.5. The resulting transient response is shown in Figure 24.

Figure 24 – Model and converter responses to a step change in duty cycle

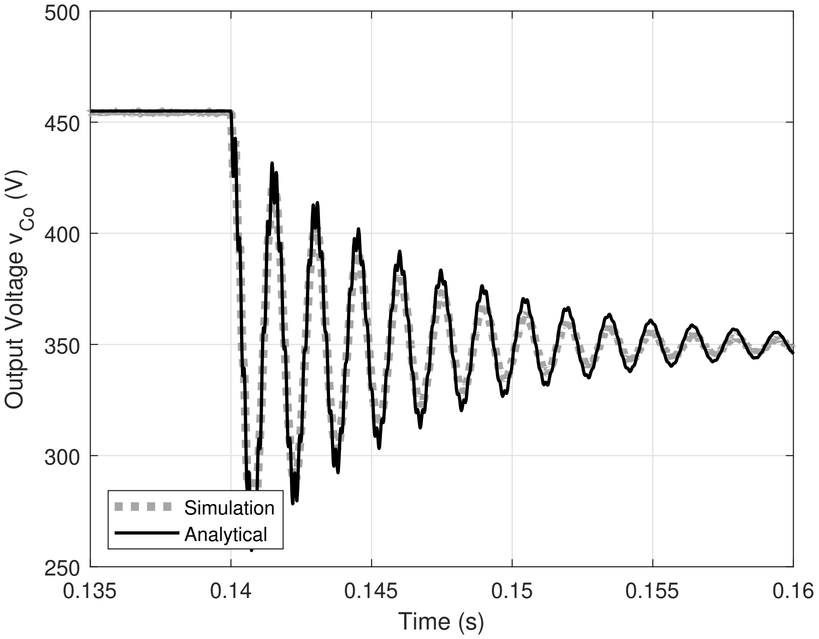

Source: The author.

5.2 Frequency-domain

To validate the proposed model, six key transfer functions of the WCR-4SSC Ćuk converter were selected. These functions relate the system's variables—the output voltage v_{Co}, the inductor 1 current i_{L1}, and the inductor 2 current i_{L2}—to perturbations in the two main inputs: the input voltage Vi and the duty cycle d. The comparison of analytical and simulated results is shown in Figure 25. The analytical expression for each transfer function is provided in Appendix B.

Figure 25 – WCR-4SSC Ćuk Transfer Functions

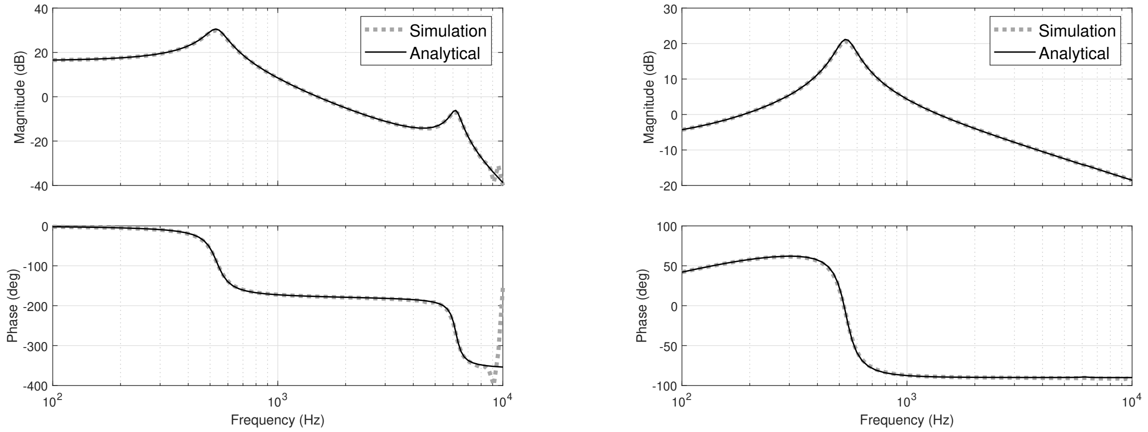

(a) $G_{vg}(s) = \frac{\hat{v_{Co}}(s)}{\hat{v}_i(s)}$ (b) $G_{i1g}(s) = \frac{\hat{i_{L1}}(s)}{\hat{v}_i(s)}$

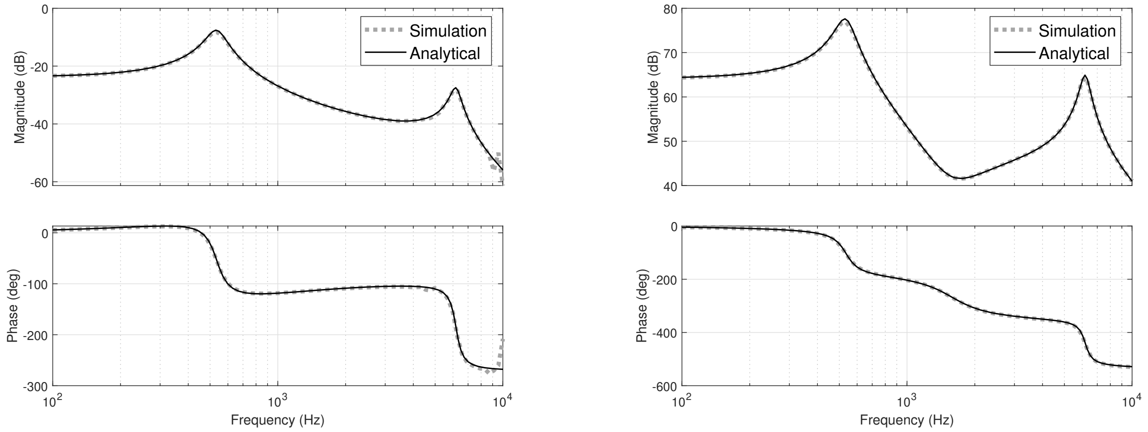

(c) $G_{i2g}(s) = \frac{\hat{i_{L2}}(s)}{\hat{v}_i(s)}$ (d) $G_{vd}(s) = \frac{\hat{v_{Co}}(s)}{\hat{d}(s)}$

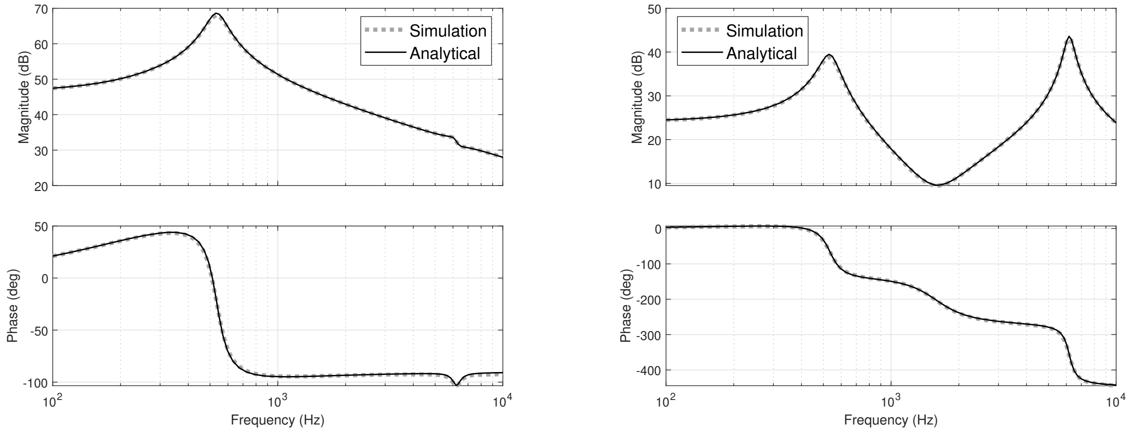

(e) $G_{i1d}(s) = \frac{\hat{i_{L1}}(s)}{\hat{d}(s)}$ (f) $G_{i2d}(s) = \frac{\hat{i_{L2}}(s)}{\hat{d}(s)}$

Source: The author.

6 CONCLUSION AND FUTURE WORKS

This work proposed a generalized modeling methodology for power converters employing the Four-State Switching Cell with Wide Conversion Range (WCR-4SSC), utilizing the state-space averaging approach. The methodology was applied to a range of classical and high-order converter topologies, providing analytical expressions of their transfer functions. By establishing a systematic modeling framework, this study contributes to the development of high-gain multiphase converters.

As the plots in the previous chapter demonstrate, the curves from the analytical model exhibit excellent agreement with the simulation data, confirming the accuracy and validity of the proposed modeling approach. The minor discrepancies observed are attributed to unmodeled parasitic elements, such as the transformer's leakage inductance.

Opportunities for future research include enhancing the model by incorporating non-ideal elements. The methodology could also be extended to the analysis of discontinuous conduction mode (DCM), with the theoretical findings validated through experimental results.

BIBLIOGRAPHY

ARAUJO, S. V.; TORRICO-BASCOPE, R. P.; TORRICO-BASCOPE, G. V. Highly efficient high step-up converter for fuel-cell power processing based on three-state commutation cell. **IEEE Transactions on Industrial Electronics**, v. 57, n. 6, p. 1987–1997, 2010.

BASCOPE, G.; BARBI, I. Generation of a family of non-isolated dc-dc pwm converters using new three-state switching cells. In: **2000 IEEE 31st Annual Power Electronics Specialists Conference. Conference Proceedings (Cat. No.00CH37018)**. [*S. l.*: *s. n.*], 2000. v. 2, p. 858–863 vol.2.

BASTOS, G. H. de A.; COSTA, L. F.; TOFOLI, F. L.; BASCOPé, G. V. T.; BASCOPé, R. P. T. Nonisolated dc–dc converters with wide conversion range for high-power applications. **IEEE Journal of Emerging and Selected Topics in Power Electronics**, v. 8, n. 1, p. 749–760, 2020.

CUK, S. **Modeling, analysis, and design of switching converters**. Tese (Doutorado) – California Institute of Technology, 1976.

ERICKSON, R.; MAKSIMOVIĆ, D. **Fundamentals of Power Electronics**. Springer International Publishing, 2020. ISBN 9783030438814. Disponível em: https://books.google.com.br/books?id=fXUmyQEACAAJ.

HONORIO, D. de A.; OLIVEIRA, D. C. P.; MOTA, E. de A.; QUEIROZ, U. R. A.; BASCOPé, R. P. T. Design and control of the wcr-4ssc boost converter on a test workbench for dc-dc converters. In: **2023 IEEE 8th Southern Power Electronics Conference and 17th Brazilian Power Electronics Conference (SPEC/COBEP)**. [*S. l.*: *s. n.*], 2023. p. 1–8.

MACIEL, W. H.; CARVALHO, J. A. R.; TOFOLI, F. L. A unified modeling approach for dc-dc converters based on the three-state switching cell. **AEU - International Journal of Electronics and Communications**, v. 88, p. 30–37, 2018. ISSN 1434-8411. Disponível em: https://www.sciencedirect.com/science/article/pii/S1434841117323555.

PERACA, M.; BARBI, I. The generation of dc-dc converters using new three-terminal multiple-state cells. In: **2005 IEEE 36th Power Electronics Specialists Conference**. [*S. l.*: *s. n.*], 2005. p. 2657–2663.

TOFOLI, F. L. Generalized pulse width modulation switch model for converters based on the multistate switching cell in discontinuous conduction mode. **Sensors**, v. 24, n. 10, 2024.

TOFOLI, F. L. Unified small-signal model for dc-dc converters based on the four-state switching cell in discontinuous conduction mode. **IEEE Journal of Emerging and Selected Topics in Power Electronics**, v. 12, n. 2, p. 1946 – 1958, 2024.

TORRICO-BASCOPE, G. V.; TORRICO-BASCOPE, R. P.; OLIVEIRA, D. S.; ANTUNES, F. L. M.; ARAUJO, S. V.; BRANCO, C. G. C. A generalized high voltage gain boost converter based on three-state switching cell. In: **IECON 2006 - 32nd Annual Conference on IEEE Industrial Electronics**. [*S. l.*: *s. n.*], 2006. p. 1927–1932.

TORRICO-BASCOPé, R. P.; COSTA, L. F.; TORRICO-BASCOPé, G. V. Generation of new nonisolated high voltage gain dc-dc converters. In: **2011 IEEE 33rd International Telecommunications Energy Conference (INTELEC)**. [*S. l.*: *s. n.*], 2011. p. 1–8.

APPENDIX A – MATLAB CODES

MATLAB code for transient analysis using the averaged state-space model

```
% --- Initialization ---
clear;
clc;
close all;

% --- Simulation Parameters ---
Tsim = 0.2;         % Total simulation time (seconds)
dt = 1e-6;          % Simulation step (seconds)

% --- Step Times ---
T1 = 0.040;          % Load step time (s)
T2 = 0.080;          % Input voltage step time (s)
T3 = 0.140;          % Duty cycle step time (s)

% --- Initial Converter Parameters ---
L1 = 135e-6;         % Inductor L1 (H)
L2 = 350e-6;         % Inductor L2 (H)
Cc = 10e-6;          % Capacitor Cc (F)
Co = 2.2e-6;         % Output Capacitor Co (F)
Ro_initial = 100;    % Initial load resistance (Ohms)
d_initial = 0.6;     % Initial duty cycle
vi_initial = 86;     % Initial input voltage (V)
N = 2;               % Transformer turns ratio

% --- New Values After Steps ---
Ro_step = 200;       % New load resistance value (Ohms)
vi_step = 70;        % New input voltage value (V)
d_step = 0.5;        % New duty cycle value

% --- Initialization of Variables that Will Change ---
Ro = Ro_initial;     % Current load resistance
```

```
vi = vi_initial;     % Current input voltage
d = d_initial;       % Current duty cycle

% Function to calculate equivalent duty cycles (assuming Region 2 for initial d)
calculate_equivalent_duty = @(d_val) deal(3*d_val - 1, 1 - (3*d_val - 1));
[deq, deq1] = calculate_equivalent_duty(d);

% Function to define state-space matrices A1 and A2
define_matrices_A = @(Ro_val, Co_val, L1_val, L2_val, Cc_val, N_val) deal(...
    [0, 0, (-1/L1_val)*(1/(3*(1+N_val))), 0; ...
     0, 0, (1/L2_val)*(1-1/(3*(1+N_val))), -1/L2_val; ...
     (1/Cc_val)*1/(3*(1+N_val)), (1/Cc_val)*(1/(3*(1+N_val))-1), 0, 0; ...
     0, 1/Co_val, 0, -1/(Ro_val*Co_val)], ... % A1 matrix for stage 1
    [0, 0, (-1/L1_val)*(2/(3*(1+N_val))), 0; ...
     0, 0, (1/L2_val)*(1-2/(3*(1+N_val))), -1/L2_val; ...
     (1/Cc_val)*2/(3*(1+N_val)), (1/Cc_val)*(2/(3*(1+N_val))-1), 0, 0; ...
     0, 1/Co_val, 0, -1/(Ro_val*Co_val)] ... % A2 matrix for stage 2
);

% --- Initial Definition of System Matrices ---
[A1, A2] = define_matrices_A(Ro, Co, L1, L2, Cc, N);

B1 = [1/L1; 0; 0; 0]; % B matrix for stage 1
B2 = [1/L1; 0; 0; 0]; % B matrix for stage 2 (same as B1 in this case)

% C matrices
```

```
C1_ = [0 0 0 1];      % C matrix for stage 1
C2_ = [0 0 0 1];      % C matrix for stage 2

% --- Initial Calculation of Average Matrices ---
A_avg = deq * A1 + deq1 * A2; % Average A matrix
B_avg = deq * B1 + deq1 * B2; % Average B matrix
C_avg = deq * C1_ + deq1 * C2_; % Average C matrix

% --- Vector Initialization ---
t = 0:dt:Tsim;              % Time vector
num_steps = length(t);      % Total number of simulation steps
num_states = size(A1, 1);   % Number of states (should be 4)
num_outputs = size(C1_, 1); % Number of outputs

x_history = zeros(num_states, num_steps); % Matrix to store state history
y_history = zeros(num_outputs, num_steps); % Matrix to store output history

% Initial Condition (zero states)
x_history(:, 1) = zeros(num_states, 1);
y_history(:, 1) = C_avg * x_history(:, 1);

% Flags to ensure steps only occur once
load_step_applied = false;
voltage_step_applied = false;
duty_step_applied = false;

% --- Simulation Loop (Forward Euler Method) ---
fprintf('Starting simulation...\n');
for k = 1:num_steps-1
    current_time = t(k);

    % 1) Load Step at T1
```

```
    if current_time >= T1 && ~load_step_applied
        Ro = Ro_step;
        [A1, A2] = define_matrices_A(Ro, Co, L1, L2, Cc, N); % Recalculate A1, A2 based on new Ro
        A_avg = deq * A1 + deq1 * A2; % Recalculate average A matrix
        % B_avg and C_avg do not depend on Ro
        load_step_applied = true;
    end

    % 2) Input Voltage Step at T2
    if current_time >= T2 && ~voltage_step_applied
        vi = vi_step;
        % No average matrices need recalculation here, only vi changes for the input term
        voltage_step_applied = true;
    end

    % 3) Duty Cycle Step at T3
    if current_time >= T3 && ~duty_step_applied
        d = d_step;
        [deq, deq1] = calculate_equivalent_duty(d); % Recalculate equivalent duty cycles
        % Recalculate all average matrices dependent on deq/deq1
        A_avg = deq * A1 + deq1 * A2;
        B_avg = deq * B1 + deq1 * B2;
        C_avg = deq * C1_ + deq1 * C2_;
        duty_step_applied = true;
    end

    % --- Calculation of Current Iteration ---
    x_current = x_history(:, k);              % Get current state vector
    x_dot = A_avg * x_current + B_avg * vi; % Calculate state
```

```
        derivatives using average model
    x_next = x_current + x_dot * dt;          % Update state
        vector using Forward Euler
    x_history(:, k+1) = x_next;               % Store the next
        state
    y_history(:, k+1) = C_avg * x_next;    %  Calculate and store
         the output for the next state


end
fprintf('Simulation finished.\n');

% --- Plot Result (Output Voltage v_Co Only) ---
figure;
plot(t, y_history, 'LineWidth', 1.5); % y_history(4,:)
   corresponds to v_Co state/output
hold on;

% Add vertical lines to indicate steps
ylim_vals = ylim; % Get current Y-axis limits to draw lines
   across the plot
plot([T1 T1], ylim_vals, 'r--', 'LineWidth', 1, 'DisplayName',
   sprintf('Load Step (%.1f Ohm)', Ro_step));
plot([T2 T2], ylim_vals, 'g--', 'LineWidth', 1, 'DisplayName',
   sprintf('Vi Step (%.1f V)', vi_step));
plot([T3 T3], ylim_vals, 'm--', 'LineWidth', 1, 'DisplayName',
   sprintf('Duty Step (%.3f)', d_step));
ylim(ylim_vals); % Restore Y-axis limits

hold off;
xlabel('Time (s)');
ylabel('Output Voltage v_{Co} (V)');
legend('show', 'Location', 'best');
grid on;
```

MATLAB code for symbolic and numerical calculation of WCR-4SSC Cuk Converter transfer functions

```
%% Choose between symbolic or numerical solution by commenting the undesired code.

%% Symbolic solution
% syms s L1 L2 Cc Co Ro Deq Vi N D;
% Deq = 3*D-1;
% I = eye(4);
%% Numerical solution
s = tf('s');
L1 = 135e-6;
L2 = 350e-6;
Cc = 10e-6;
Co = 2.2e-6;
Ro = 100;
D = 0.6;
Deq = 3*D-1;
Vi = 86;
N = 2;

I = eye(4);
%% 0 < t <= DT
A1 = [0                     0                       (-1/L1)*(1/(3*(1+N)))       0;
      0                     0                       (1/L2)*(1-1/(3*(1+N)))      -1/L2;
      (1/Cc)*1/(3*(1+N))    (1/Cc)*(1/(3*(1+N))-1)  0                           0;
      0                     1/Co                    0                           -1/(Ro*Co)];

B1 = [1/L1; 0; 0; 0];
C1_ = [1 0 0 0; 0 1 0 0; 0 0 1 0; 0 0 0 1];
```

```
%% DT < t <= T
A2 = [0                     0                       (-1/L1)*(2/(3*(1+N)))       0;
      0                     0                       (1/L2)*(1-2/(3*(1+N)))      -1/L2;
      (1/Cc)*2/(3*(1+N))    (1/Cc)*(2/(3*(1+N))-1)  0                           0;
      0                     1/Co                    0                           -1/(Ro*Co)];

B2 = [1/L1; 0; 0; 0];
C2_ = [1 0 0 0; 0 1 0 0; 0 0 1 0; 0 0 0 1];
%% Average model
A = Deq*A1 + (1-Deq)*A2;
B = Deq*B1 + (1-Deq)*B2;
C_ = Deq*C1_ + (1-Deq)*C2_;

X = -inv(A)*B*Vi;
Y = -C_*inv(A)*B*Vi;
%% Transfer functions
y_vi = C_*inv(s*I-A)*B;
y_d = 3*(C_*inv(s*I-A)*((A1-A2)*X+(B1-B2)*Vi)+(C1_-C2_)*X);

il1_d = y_d(1);
il2_d = y_d(2);
vo_d = y_d(4);
il1_vi = y_vi(1);
il2_vi = y_vi(2);
vo_vi = y_vi(4);
```

APPENDIX B – TRANSFER FUNCTIONS FOR CLASSICAL TOPOLOGIES (REGION 2)

Although the main analysis in this work centered on the WCR-4SSC Ćuk converter, the cell can be integrated with all classical topologies to create a new family of power converters (BASTOS *et al.*, 2020), as shown in Figure 26. This appendix summarizes the complete set of transfer functions for this family, derived for operation in Region 2.

Where N is the transformer turns ratio, V_i is the input voltage, $L1$ is the input filter, Co is the output filter capacitor, Cc is the coupling capacitor, and Ro is the load.

For second-order converters, including the Buck, Boost, and Buck-Boost topologies, it is common practice to express their transfer functions in terms of poles and zeros, as indicated in Equations B.1a-B.1d.

$$G_{vd}(s) = \frac{\hat{v_{Co}}(s)}{\hat{d}(s)} = G_{vd0} \cdot \frac{1 - \dfrac{s}{w_{z1}}}{1 + \dfrac{s}{Qw_0} + \left(\dfrac{s}{w_0}\right)^2} \tag{B.1a}$$

$$G_{id}(s) = \frac{\hat{i_L}(s)}{\hat{d}(s)} = G_{id0} \cdot \frac{1 - \dfrac{s}{w_{z2}}}{1 + \dfrac{s}{Qw_0} + \left(\dfrac{s}{w_0}\right)^2} \tag{B.1b}$$

$$G_{vg}(s) = \frac{\hat{v_{Co}}(s)}{\hat{v_i}(s)} = G_{vg0} \cdot \frac{1}{1 + \dfrac{s}{Qw_0} + \left(\dfrac{s}{w_0}\right)^2} \tag{B.1c}$$

$$G_{ig}(s) = \frac{\hat{i_L}(s)}{\hat{v_i}(s)} = G_{ig0} \cdot \frac{1 - \dfrac{s}{w_{z3}}}{1 + \dfrac{s}{Qw_0} + \left(\dfrac{s}{w_0}\right)^2} \tag{B.1d}$$

Where $G_{vd0}, G_{id0}, G_{vg0}$ and G_{ig0} are the DC gain of the respective transfer function, Q is the quality factor, w_0 is the natural frequency, and w_z is the zero frequency. Tables 4 and 5 provide a summary of the corresponding coefficients, where $D_1 = 1 - D$.

Figure 26 – WCR-4SSC dc-dc converters

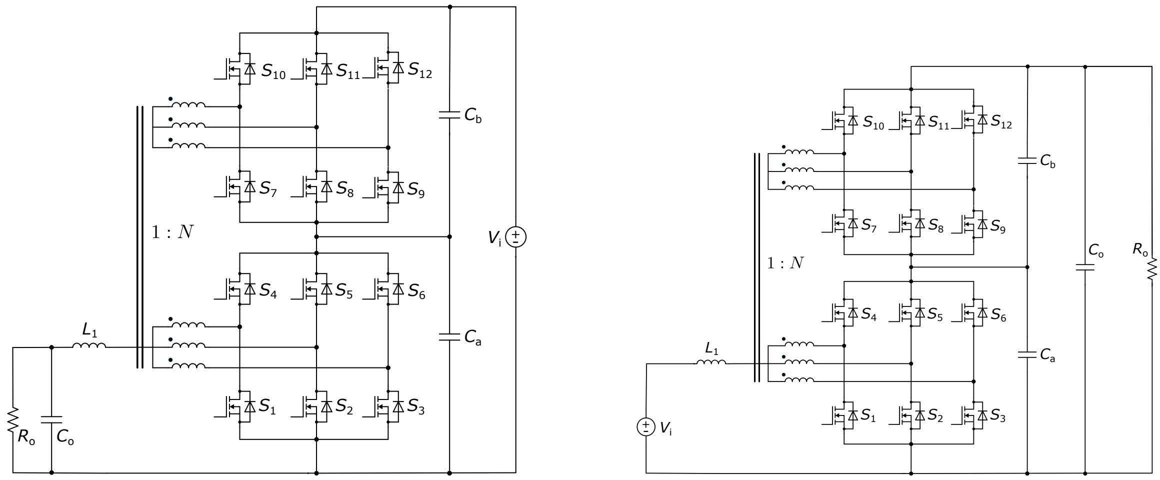

(a) WCR-4SSC Buck (b) WCR-4SSC Boost

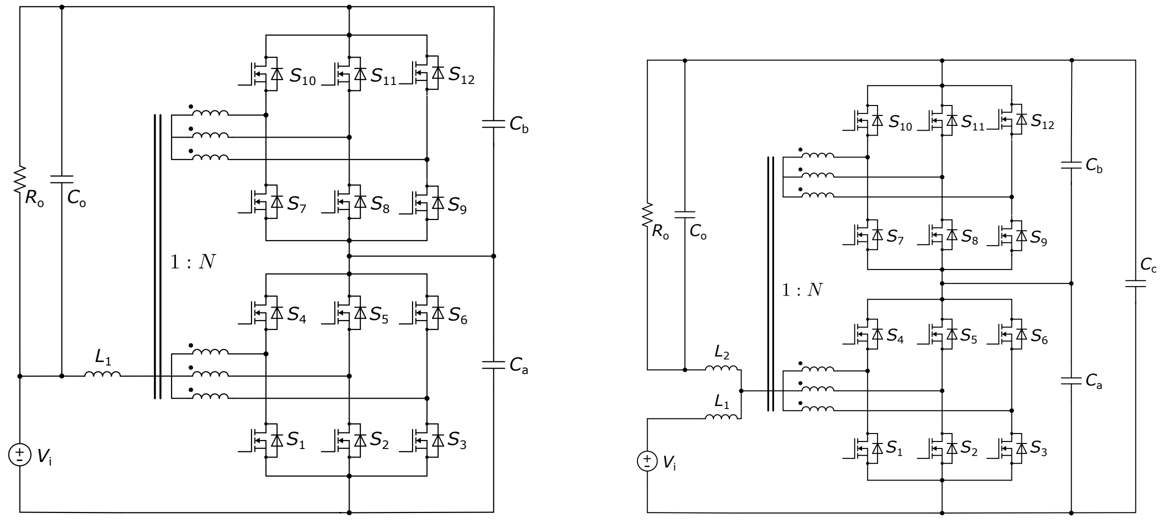

(c) WCR-4SSC Buck-Boost (d) WCR-4SSC Ćuk

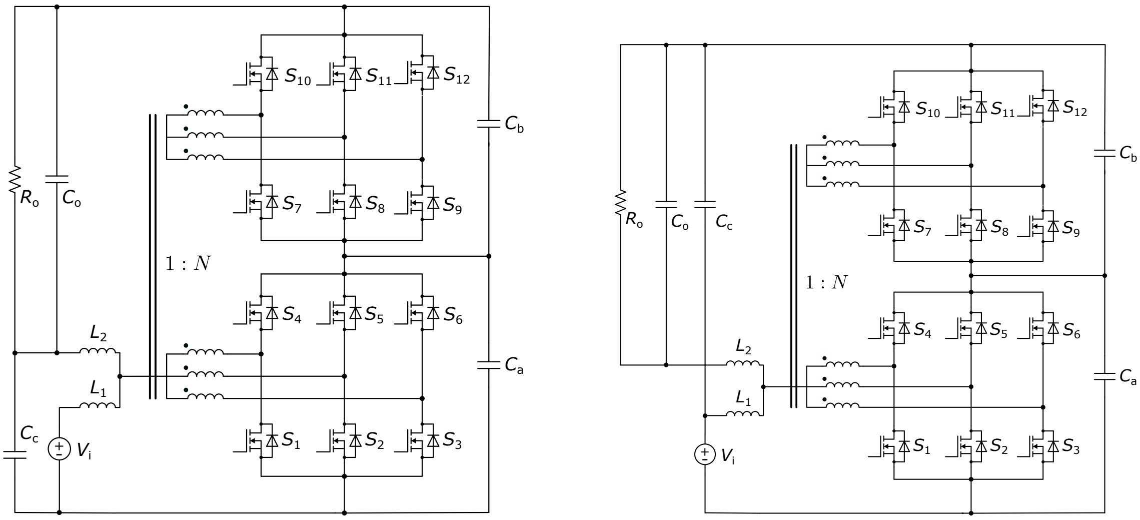

(e) WCR-4SSC SEPIC (f) WCR-4SSC Zeta

Source: Adapted from (BASTOS *et al.*, 2020).

Table 4 – Gains (2nd order converters)

Converter	G_{vd0}	G_{id0}	G_{vg0}	G_{ig0}
Buck	$\frac{-1}{N+1} \cdot Vi$	$\frac{-1}{N+1} \cdot \frac{Vi}{Ro}$	$\frac{D_1}{N+1}$	$\frac{D_1}{(N+1)Ro}$
Boost	$\frac{N+1}{{D_1}^2} \cdot Vi$	$\frac{2(N+1)^2}{{D_1}^2} \cdot \frac{Vi}{RoD_1}$	$\frac{N+1}{D_1}$	$\frac{(N+1)^2}{{D_1}^2 Ro}$
Buck-Boost	$\frac{N+1}{{D_1}^2} \cdot Vi$	$\frac{(2N+1+D)(N+1)}{{D_1}^2} \cdot \frac{Vi}{RoD_1}$	$\frac{N+D}{D_1}$	$\frac{(N+1)(N+D)}{{D_1}^2 Ro}$

Source: The author.

Table 5 – Poles and Zeros Frequencies (2nd order converters)

Converter	Q	w_0	w_{z1}	w_{z2}	w_{z3}
Buck	$Ro\sqrt{\frac{Co}{L1}}$	$\frac{1}{\sqrt{L1 \cdot Co}}$	∞	$\frac{-1}{RoCo}$	$\frac{-1}{RoCo}$
Boost	$\frac{-D_1}{(N+1)} \cdot Ro\sqrt{\frac{Co}{L1}}$	$\frac{-D_1}{(N+1)} \cdot \frac{1}{\sqrt{L1 \cdot Co}}$	$\frac{D_1^2}{(N+1)^2} \cdot \frac{Ro}{L1}$	$\frac{-2}{RoCo}$	$\frac{-1}{RoCo}$
Buck-Boost	$\frac{-D_1}{(N+1)} \cdot Ro\sqrt{\frac{Co}{L1}}$	$\frac{-D_1}{(N+1)} \cdot \frac{1}{\sqrt{L1 \cdot Co}}$	$\frac{D_1^2}{(N+1)(N+D)} \cdot \frac{Ro}{L1}$	$\frac{-(2N+D+1)}{(N+1) \cdot RoCo}$	$\frac{-1}{RoCo}$

Source: The author.

For fourth-order converters, the transfer functions assume the following general form:

$$G_{vd}(s) = \frac{\hat{v_{Co}}(s)}{\hat{d}(s)} = G_{vd0} \cdot \frac{a_3 \cdot s^3 + a_2 \cdot s^2 + a_1 \cdot s + 1}{g_4 \cdot s^4 + g_3 \cdot s^3 + g_2 \cdot s^2 + g_1 \cdot s + 1} \tag{B.2a}$$

$$G_{i1d}(s) = \frac{\hat{i_{L1}}(s)}{\hat{d}(s)} = G_{i1d0} \cdot \frac{b_3 \cdot s^3 + b_2 \cdot s^2 + b_1 \cdot s + 1}{g_4 \cdot s^4 + g_3 \cdot s^3 + g_2 \cdot s^2 + g_1 \cdot s + 1} \tag{B.2b}$$

$$G_{i2d}(s) = \frac{\hat{i_{L2}}(s)}{\hat{d}(s)} = G_{i2d0} \cdot \frac{c_3 \cdot s^3 + c_2 \cdot s^2 + c_1 \cdot s + 1}{g_4 \cdot s^4 + g_3 \cdot s^3 + g_2 \cdot s^2 + g_1 \cdot s + 1} \tag{B.2c}$$

$$G_{vg}(s) = \frac{\hat{v_{Co}}(s)}{\hat{v}_i(s)} = G_{vg0} \cdot \frac{d_2 \cdot s^2 + 1}{g_4 \cdot s^4 + g_3 \cdot s^3 + g_2 \cdot s^2 + g_1 \cdot s + 1} \tag{B.2d}$$

$$G_{i1g}(s) = \frac{\hat{i_{L1}}(s)}{\hat{v}_i(s)} = G_{i1g0} \cdot \frac{e_3 \cdot s^3 + e_2 \cdot s^2 + e_1 \cdot s + 1}{g_4 \cdot s^4 + g_3 \cdot s^3 + g_2 \cdot s^2 + g_1 \cdot s + 1} \tag{B.2e}$$

$$G_{i2g}(s) = \frac{\hat{i_{L2}}(s)}{\hat{v}_i(s)} = G_{i2g0} \cdot \frac{f_3 \cdot s^3 + f_2 \cdot s^2 + f_1 \cdot s + 1}{g_4 \cdot s^4 + g_3 \cdot s^3 + g_2 \cdot s^2 + g_1 \cdot s + 1} \tag{B.2f}$$

The coefficients are summarized in Tables 6-9.

Table 6 – Gains (4th order converters)

Coefficients	Ćuk	SEPIC	Zeta
G_{vd0}		$\frac{N+1}{{D_1}^2} \cdot Vi$	
G_{i1d0}	$2(N+1)(N+D) \cdot Vi$	$\frac{2(N+1)(N+D)}{Ro{D_1}^3} \cdot Vi$	$\frac{2(N+1)(N+D)}{Ro{D_1}^3} \cdot Vi$
G_{i2d0}		$\frac{N+1}{Ro{D_1}^2} \cdot Vi$	
G_{vg0}		$\frac{N+D}{D_1}$	
G_{i1g0}		$\frac{(N+D)^2}{Ro{D_1}^2}$	
G_{i2g0}		$\frac{N+D}{RoD_1}$	

Source: The author.

Table 7 – Coefficients for control-to-output transfer functions (4th order converters)

Coefficients	Ćuk	SEPIC	Zeta
a_3	0	$-(N+D)(N+1)\cdot\dfrac{CcL1L2}{RoD_1{}^2}$	0
a_2	$(N+1)\cdot\dfrac{CcL1}{D_1}$	$Cc(L1+L2)$	$(N+1)\cdot\dfrac{CcL1}{D_1}$
a_1		$-(N+D)^2\cdot\dfrac{L1}{RoD_1{}^2}$	
b_3		$\dfrac{N+1}{2(N+D)}\cdot CcCoL2Ro$	
b_2	$L2\left[\dfrac{N+1}{2(N+D)}Cc+\dfrac{Co}{2}\right]$	$L2\left[\dfrac{2N+D+1}{2(N+D)}Cc+\dfrac{Co}{2}\right]$	$L2\left[\dfrac{N+1}{2(N+D)}Cc+\dfrac{Co}{2}\right]$
b_1	$\dfrac{L2}{2Ro}+\dfrac{RoCo}{2}+\left(\dfrac{N+1}{N+D}\right)\dfrac{RoCc}{2}$	$\dfrac{L2}{2Ro}+\dfrac{RoCo}{2}$	$\dfrac{L2}{2Ro}+\dfrac{RoCo}{2}+\left(\dfrac{N+1}{N+D}\right)\dfrac{RoCc}{2}$
c_3		$(N+1)\dfrac{CcCoL1Ro}{D_1}$	
c_2	$L1\left[\dfrac{N+1}{D_1}\cdot Cc-\dfrac{(N+D)^2}{D_1{}^2}\cdot Co\right]$	$L1\left[\dfrac{2(N+1)+D_1}{D_1}\cdot Cc-\dfrac{(N+D)^2}{D_1{}^2}\cdot Co\right]$	$L1\left[\dfrac{N+1}{D_1}\cdot Cc-\dfrac{(N+D)^2}{D_1{}^2}\cdot Co\right]$
c_1		$RoCo-\dfrac{(N+D)^2}{D_1{}^2}\dfrac{L1}{Ro}$	

Source: The author.

Table 8 – Coefficients for the voltage input-to-output transfer functions (4th order converters)

Coefficients	Ćuk	SEPIC	Zeta
d_2	0	$\frac{N+1}{N+D} \cdot CcL2$	$\frac{N+1}{D_1} \cdot CcL1$
e_3	$\frac{(N+1)^2}{(N+D)^2} \cdot CcCoL2Ro$	$\frac{(N+1)^2}{(N+D)^2} \cdot CcCoL2Ro$	$\frac{N+1}{N+D} \cdot CcCoL2Ro$
e_2	$\frac{(N+1)^2}{(N+D)^2} \cdot CcL2$	$\frac{(N+1)^2}{(N+D)^2} \cdot CcL2$	$\frac{N+1}{N+D} \cdot CcL2$
e_1	$\frac{(N+1)^2}{(N+D)^2} \cdot RoCc + RoCo$	$\frac{{D_1}^2}{(N+D)^2} \cdot RoCc + RoCo$	$\frac{N+1}{N+D} \cdot RoCc + RoCo$
f_3	0	0	$\frac{N+1}{D_1} \cdot CcCoL1Ro$
f_2	0	0	$\frac{N+1}{D_1} \cdot CcL1$
f_1	$RoCo$	$\frac{-D_1}{N+D} \cdot RoCc + RoCo$	$RoCo$

Source: The author.

Table 9 – Coefficients of the denominators of the transfer functions (4th order converters)

Coefficients	Ćuk	SEPIC	Zeta
g_4	$\frac{(N+1)^2}{{D_1}^2} \cdot CcCoL1L2$		
g_3	$\frac{(N+1)^2}{Ro{D_1}^2} \cdot CcL1L2$		
g_2	$L1\left[\frac{(N+1)^2}{{D_1}^2}Cc + \frac{(N+D)^2}{{D_1}^2}Co\right]$ $+CoL2$	$L1\left[Cc + \frac{(N+D)^2}{{D_1}^2}Co\right]$ $+(Cc+Co)L2$	$L1\left[\frac{(N+1)^2}{{D_1}^2}Cc + \frac{(N+D)^2}{{D_1}^2}Co\right]$ $+\frac{CoL2}{D_1}$
g_1	$L1\left[\frac{(N+D)^2}{Ro{D_1}^2}\right] + \frac{L2}{Ro}$		

Source: The author.

APPENDIX C – PSIM SCHEMATIC

Figure 27 – PSIM circuit used for simulations.

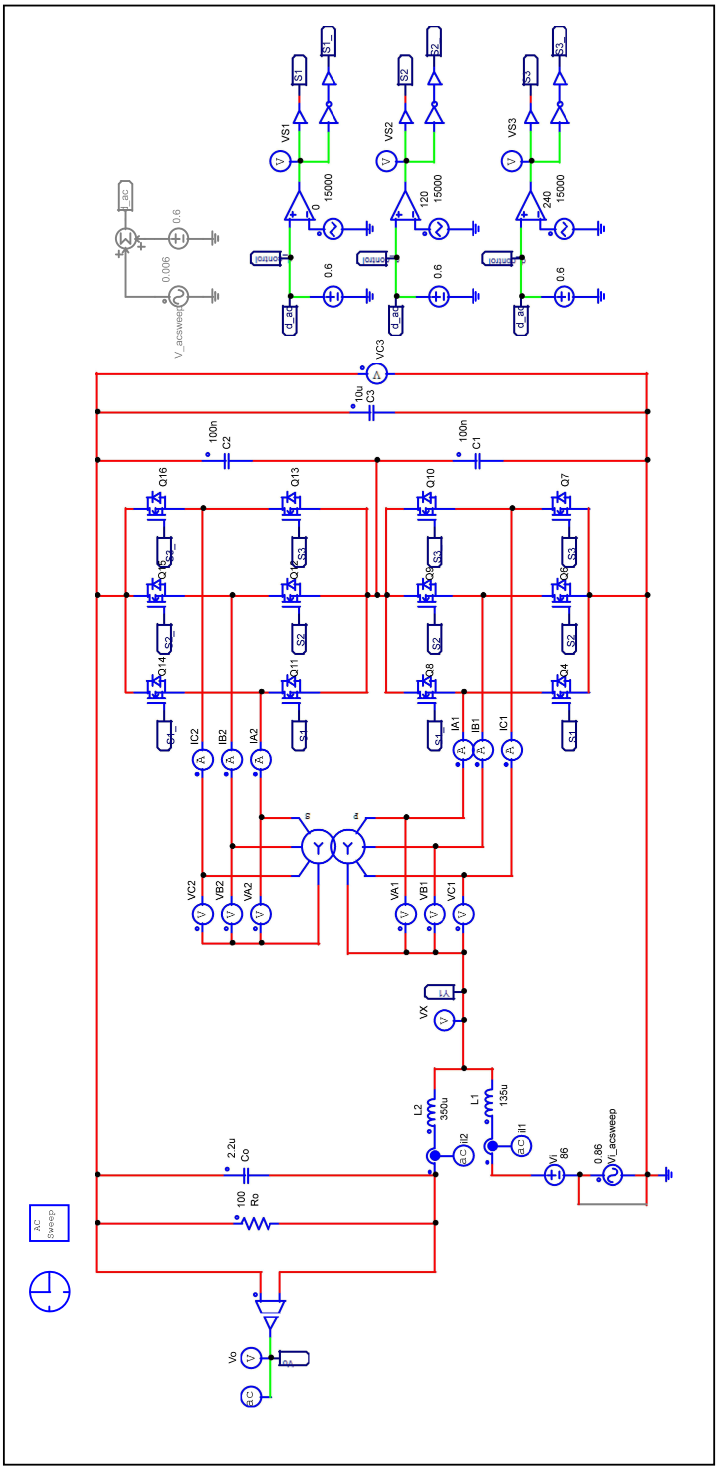

Source: The author.